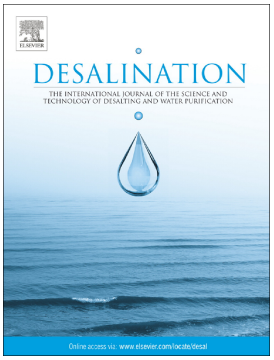

Venturi nozzles for desalination brine discharges

Niki Soleimani Amiri, Ozeair Abessi, Philip J.W. Roberts

PII: S0011-9164(23)00825-1

DOI: https://doi.org/10.1016/j.desal.2023.117193

Reference: DES 117193

To appear in: *Desalination*

Received date: 10 July 2023

Revised date: 21 November 2023

Accepted date: 26 November 2023

Please cite this article as: N.S. Amiri, O. Abessi and P.J.W. Roberts, Venturi nozzles for desalination brine discharges, *Desalination* (2023), https://doi.org/10.1016/j.desal.2023.117193

Venturi nozzles for desalination brine discharges

Niki Soleimani Amiri[1], Ozeair Abessi[2*], Philip J. W. Roberts[3]

1.MSc. Student, Department of Civil Engineering, Babol Noshirvani University of Technology, Babol, Iran
nikisoleimani1997@gmail.com
2. Associate Professor, Department of Civil Engineering, Babol Noshirvani University of Technology, Babol, Iran
(*Corresponding author: Oabessi@nit.ac.ir)
3. Professor, School of Civil and Environmental Engineering, Georgia Institute of Technology, Atlanta, GA 30332, USA;
phil.roberts@ce.gatech.edu

Abstract

Seawater desalination is a reliable way to confront the growing challenges of freshwater demands in the world. Brine is the primary by-product of this process and needs to be carefully managed and discharged back into the sea. In coastal desalination plants, the use of submerged outfall as a pipeline laying on the ocean floor is a popular strategy to minimize the environmental impacts of brine discharge. The Venturi nozzle has been proposed as a more efficient method for dispersing brine into the ocean. However, it requires a high exit velocity, which poses limitations for steep nozzle angles in shallow waters. This study aims to investigate the benefits of a lower range of exit velocities in the Venturi nozzles. The 60° inclined dense jet from a Venturi nozzle was explored, numerically and experimentally, and the results were compared to those of a simple dense jet. Comparisons showed that the Venturi nozzle decreases the flow path and diminishes flow dilution at the critical points. However, this reduction can be compensated by increasing the discharge Froude number to reach the same trajectory as a simple jet. It is important to note that this compensation is intricately linked to the discharge velocity, and it makes the use of Venturi nozzles for brine discharge a challenging proposition in both deep and shallow waters.

Keywords: Desalination, Brine disposal, Venturi nozzle, Inclined dense discharge, Mixing zone.

List of symbols

x_i	i_{th} coordinate direction	u_i	Filtered velocity in i direction
x_j	j_{th} coordinate direction	u_j	Filtered velocity in j direction
g	Gravitational acceleration	x_m	Horizontal component of jet centerline peak
g'	Reduced gravitational acceleration	y_m	Vertical component of jet centerline peak
Fr_d	Densimetric Froude number	y_t	Terminal rise height
L_M	Momentum-buoyancy length scale	x_r	Horizontal distance of return point
L_Q	Discharge length scale	x_i	Horizontal distance of impact point
d	Nozzle diameter	S_i	Impact point dilution
ρ_0	Effluent density	S_r	Return point dilution
ρ_a	Ambient density	C_0	Jet discharge concentration
ρ	Fluid density	C	Local concentration
U	Jet velocity	C_{max}	Maximum concentration at the jet maximum height
θ	Discharge angle	Q_0	Jet discharge volume flux
t	Time	M_0	Momentum flux
T^*	Non-dimensionalized time	B_0	Buoyancy flux
b	Jet flow width	Δ	Effective width
L_{Cl}	Flow path length	$\bar{p}_{rgh}$	Filtered dynamic pressure
ν_{SGS}	Sub-Grid Scale kinematic viscosity	υ	Molecular kinematic viscosity
$\bar{S}_{ij}$	Strain-rate tensor	υ_e	Effluent molecular kinematic viscosity
D_{ab}	Molecular diffusivity	υ_a	Ambient molecular kinematic viscosity
Sc_{SGS}	Turbulent Schmidt number	α	Volume fraction of effluent

List of abbreviation

LA	Light Attenuation
LIF	Laser Induced Fluorescence
PIV	Particle Image Velocimetry
PTV	Particle Tracking Velocimetry
LES	Large Eddy Simulation
PLIF	Planar Laser-Induced Fluorescence
VNExp	Venturi Nozzle Experiment (LIF)
SNExp	Simple Nozzle Experiment (LIF)
Exp	Experimental study
Num	Numerical study

1. Introduction

Population growth, agricultural expansion, and environmental changes have resulted in water scarcity in many parts of the world. This has led to a rapid growth in the global demand for freshwater, particularly in coastal cities in the arid areas of the Middle East. Seawater desalination has gained worldwide acceptance as a reliable solution to address this growing demand during the last decade (Hoekstra 2014; Abessi 2018). In desalination plants, large volumes of freshwater are produced from seawater, and their main by-product, brine, is

discharged back into the sea. If the brine is adequately diluted in the receiving water, it can be safely disposed of. Submerged outfalls are a commonly employed practice to ameliorate the negative impacts of brine on marine ecosystems (Roberts and Abessi 2014). In particular, the inclined discharge has been proposed for the disposal of brine because it prevents flow from falling back directly onto itself. The steep angle to the horizontal plane aids the flow to go a longer path, and it increases the chance of the flow to reach better dilution. Therefore, brine can effectively mix with the surrounding water, and it facilitates rapid the reduction of potentially toxic materials to the safe levels (Abessi and Roberts 2015, 2018).

The circular and simple nozzles have been the common geometries in most prior research. Therefore, so far several experimental and numerical studies have been conducted to investigate the dynamics and mixing of circular dense jets under various conditions. The earliest studies on this topic were reported by Cederwall (1968), Zeitoun et al. (1970), and Roberts et al. (1987). These studies aimed to determine the optimal angle of inclination for brine discharge. Zeitoun et al. (1970) conducted experiments measuring dilution at different angles and concluded that a 60° nozzle creates the longest trajectory and likely maximum dilution among the different angles. Roberts et al. (1997) performed comprehensive experimental research on 60° inclined dense jets to disclose flow behavior in the near-field region. To further characterize the prominent features of inclined dense jets, recent laboratory studies have employed novel experimental techniques such as Light Attenuation (LA), Laser Induced Fluorescence (LIF), Particle Image Velocimetry (PIV), and Particle Tracking Velocimetry (PTV). Kikkert et al. (2007) used LA techniques to demonstrate that maximum dilution occurs at the return point for a 60° angle. Lai and Lee (2012), based on comprehensive LIF and PIV experiments, showed that the angle of the nozzle within the range of 38° to 60° inclination does not significantly affect dilution at the point of bottom impingement. Oliver et al. (2013) proposed a novel analytical approach to determine dilution throughout the range of 15° to 75° for dense jets. As an ablation study, they showed that the analytical solution can produce more accurate results and predictions compared to other techniques. Considering various single dense jets at 15°-85° angles, Abessi and Roberts (2015) demonstrated that dilution at the impact point remains relatively unchanged when the nozzle angle varies between 45° and 60°. Slightly better dilution, however, was observed at the end of the near field for a 60° angle. Crowe et al. (2016) employed PTV techniques to quantify flow velocity distribution in dense jets with angles ranging from 15° to 75°. Generally, these studies have focused on the flow dilution and geometrical characteristics at critical points for commonly used angles. Additionally, Papakonstantis and Tsatsara (2019) investigated flow behavior in dense jets with angles of 25°, 50°, and 70°.

Besides experimental studies, more recently, numerical studies have adopted Computational Fluid Dynamics (CFD) tools, such as OpenFOAM and Ansys Fluent, to simulate dense jet characteristics under different circumstances. Vafeiadou et al. (2005) employed the k-ω Shear Stress Transport (SST) turbulence model to numerically simulate dense jets at 60° in stagnant waters. The model underestimates both the terminal rise height and the return point compared to the experimental observations. Oliver et al. (2008) used the CFX package to execute a series of simulations on the inclined dense jet to identify an optimal turbulent Schmidt number in the standard k-ε turbulence model. Gildeh et al. (2015) used RNG k-ε, realizable k-ε, nonlinear k-ε, LRR, and Lunder-Gibson turbulence models to investigate the geometrical and mixing properties of inclined dense jets in stationary environments. According to this study, the LRR and realizable k-ε models provide more accurate predictions for the geometrical characteristics compared to the other models. Ramezani et al. (2021) employed the Reynolds-Averaged Navier-Stokes (RANS)

approach and the realizable k-ε turbulence model to analyze the effect of proximity to the bed in both 30° and 45° inclined dense jets. The numerical results demonstrated that the model could successfully predict the geometrical characteristics of dense jets, while the dilution predictions were conservative.

The large Eddy Simulation (LES) method contains more information than the RANS models and only recently its potential has been explored for the brine discharge simulations. Zhang et al. (2017) conducted an LES study to model the behavior of dense jets at 45° and 60° angles. The model predicted the behavior of dense jets with better accuracy compared to RANS models; Nevertheless, it underestimated the impact point dilution in relation to the experiments. Tofighian et al. (2022) also developed a comprehensive LES study to investigate flow behavior in 15°, 30°, 45°, 60°, and 75° inclined dense jets. They focused on the near-wall region and performed several experiments with the Planar Laser-Induced Fluorescence (PLIF) techniques to verify the LES results. Based on the comparisons, the numerical model was able to estimate the mixing and geometrical properties of the concentrated jets with up to 25% underestimation.

Besides circular jets, using non-circular nozzles has also been investigated for the flow discharges by Gutmark and Grinstein (1999), Mi et al. (2000), and Portillo et al. (2013). Lee et al. (1998), Lee et al. (2001) and Wang et al. (2012) focused on the hydraulics of duckbill valves in non-circular nozzle geometries. Jiang et al. (2019) experimentally investigated the behavior of a 45° inclined dense jet with various geometries of the nozzle, including circular, square, duckbill, star, and diamond shapes, focusing on the flow mixing and dilution. They also developed an LES model with the Dynamic Smagorinsky sub-grid model to analyze the performance of the diamond, duckbill, and star-shaped nozzle geometries. According to the experimental results, the duckbill and star-shaped nozzle geometries demonstrated greater levels of dilution at both the centerline peak and return point. The numerical results also proved that the dilution was underestimated by about 25% in comparison to the experimental results. This discrepancy highlights the need for further improvement in the dilution calculations.

Overall, previous studies lacked experimental and numerical analysis of complex nozzle geometries. In a different set of investigations, Portillo et al. (2013) used the Venturi nozzle for a 15^{o} inclined dense jet to improve dilution in the Maspalomas II desalination discharge system in the Canary Islands, Spain. It was crucial there to preserve the Cymodocea nodosais, the island's largest and most ecologically significant seagrass meadow. Using Venturi diffusers instead of the conventional nozzles is assumed to enhance brine dilution at this point. By measuring salinities at a fixed location over several days, they reported that the Venturi nozzles could reach higher dilution than conventional diffusers due to pre-dilution that happens at the Venturi eductor. Measuring dilution in the field is quite difficult and is not a good basis for assessing the advantage of the Venturi device. Therefore, there are not adequate measurements for analyzing the efficiency of the Venturi nozzles. The carefully controlled laboratory experiments with and without the Venturi nozzle are better ways to measure the devices' effectiveness.

Hence, in this study, a Venturi nozzle with 60° inclination is numerically simulated using the LES method. A series of experimental simulations was also conducted using the LIF techniques to verify the numerical results. In addition, a simple nozzle was modeled to compare with the Venturi nozzle data and quantify the LES predictions' accuracy. The key objective is to determine the possible extent of enhancement in flow mixing in the Venturi nozzle compared to the simple nozzle for lower exit velocity in both mathematical and laboratory simulations. Trajectory, flow widths, and mixing characteristics were therefore determined.

2. Materials and Methods

2.1 Governing equations

There are three main methods in the simulation of turbulent flow, namely Direct Numerical Simulation (DNS), Large Eddy Simulation (LES), and Reynolds-Averaged Navier-Stokes (RANS). DNS is the most accurate and computationally expensive method that captures the smallest eddies up to the flow regime's largest eddies. In LES, only small-scale eddies of the flow are modeled, whereas larger eddies are computed directly. The lower computational cost of the LES method compared to DNS, makes it an efficient tool for predicting the characteristics of the turbulent flows. The time-averaged equations of motion for fluid flow, i.e., RANS models, represent the mean of all turbulent motions. According to its low computational costs, this method has been the basis for industrial CFD applications in the past few decades. Although it has shown adequate preciseness in industrial applications, it cannot predict the flow behavior in complicated geometries and problems (Zhiyin 2015). While, previous studies have demonstrated the capacity of the LES for complex geometry and realistic problems (Tofighian et al. 2022). In the LES model, eddies are sorted into two classes, large and small, by utilizing the local grid sizes as a filtering criterion. After filtering, the large eddies are computed directly using the instantaneous Navier-Stokes equations. On the other hand, smaller eddies are modeled using certain assumptions, such as the Boussinesq hypothesis. The mass and momentum conservation equations for an incompressible multiphase flow are the governing equations, and OpenFOAM numerically solves them using the finite volume method. The following formulas refer to the filtered three-dimensional unsteady Navier–Stokes equations for incompressible flows, which are derived using an implicit filter represented by the operator "-", with an effective width of $\Delta = (V_c)^{1/3}$ (Zhang et al. 2016).

$$\frac{\partial \bar{u}_j}{\partial x_j} = 0 \quad (1)$$

$$\frac{\partial(\rho\bar{u}_i)}{\partial t} + \frac{\partial(\rho\bar{u}_i\bar{u}_j)}{\partial x_j} = -\frac{\partial \bar{p}_{rgh}}{\partial x_i} - gh\frac{\partial \rho}{\partial x_i} + \frac{\partial}{\partial x_i}[2\rho(\upsilon + \nu_{SGS})\bar{S}_{ij}] \quad (2)$$

Where u_i and u_j represent the filtered velocity in i and j direction, g denotes the acceleration due to gravity, x_i and x_j are the i_{th} and j_{th} coordinate direction, t is the time, $\bar{p}_{rgh}$ is the filtered dynamic pressure, ν_{SGS} is the Sub-Grid Scale (SGS) kinematic viscosity and is utilized to simulate the influence of SGS fluctuations through a diffusive mechanism, h corresponds to the height of the fluid column and $\bar{S}_{ij}$ is the strain-rate tensor.

ρ and υ represent the density and molecular kinematic viscosity of the mixture, respectively. The values of ρ and υ are calculated using the following equations:

$$\rho = \alpha\rho_e + (1-\alpha)\rho_a \quad (3)$$

$$\upsilon = \alpha\upsilon_e + (1-\alpha)\upsilon_a \quad (4)$$

Where α is the volume fraction of effluent and is calculated using a transport equation, which is formulated below. Moreover, ρ_e stands for effluent density, υ_e denotes effluent molecular kinematic viscosity, while ρ_a and υ_a are ambient density and ambient molecular kinematic viscosity, respectively.

$$\frac{\partial \bar{\alpha}}{\partial t} + \frac{\partial (\bar{u}_j \bar{\alpha})}{\partial x_j} = \frac{\partial}{\partial x_j}[\left(D_{ab} + \frac{\upsilon_{SGS}}{Sc_{SGS}}\right)\frac{\partial \bar{\alpha}}{\partial x_j}] \quad (5)$$

In the above equation, D_{ab} is the molecular diffusivity and Sc_{SGS} is the turbulent Schmidt number. The parameter υ_{SGS} which is defined earlier, is calculated within the LES model through a one-equation SGS kinetic energy, k_{SGS}, transport model as described by Tofighian et al. (2020):

$$\upsilon_{SGS} = C_k \bar{\Delta} k_{SGS}^{1/2} \quad (6)$$

$$\frac{\partial k_{SGS}}{\partial t} + \frac{\partial (\bar{u}_j k_{SGS})}{\partial x_j} = \upsilon_{SGS}\left(2\bar{S}_{ij}\bar{S}_{ij}\right) - C_\varepsilon k_{SGS}^{\frac{3}{2}}/\bar{\Delta} + \frac{\partial}{\partial x_j}(\upsilon_{SGS}\frac{\partial k_{SGS}}{\partial x_j}) \quad (7)$$

In this case, the dynamic LES model, as introduced by Kim and Menon (1995), utilized a test filter with a doubled length, $\tilde{\Delta} = 2\bar{\Delta}$, for the computation of C_k and C_ε.

2.2 Numerical Methods and Computational Setup

OpenFOAM (version 6) as an open-source software package was utilized in this study. The twoLiquidMixingFoam solver has been chosen and used for the mixture flow of two incompressible fluids. This solver uses a PIMPLE algorithm, which is a combination of the SIMPLE and PISO algorithms, to solve the pressure-velocity coupled equations (Zhang et al. 2017). Higher Courant numbers and larger time steps are possible using the PIMPLE algorithm.

In the developed LES model, the second-order backward method is applied to discretize temporal terms. The diffusion terms were discretized by using the second-order linear method. This method is not suitable for the discretization of transition terms due to the production of non-physical fluctuations. Therefore, the transition terms have been discretized by the Gauss filtered Linear method, a second-order linear method in OpenFOAM. To discretize the transfer equation of the volume fraction, Van Leer's second-order method was applied. Also, for U, K, ω, C, and $\bar{p}_{rgh}$, the convergence criterion of 10^{-6} is set.

A schematic view of the computational domain with dimensions of 1.5 m long, 0.8 m wide, and 1.03 m deep is shown in Fig. 1. The angle of discharge is set at 60° to the horizontal plane, and 1.3 m and 0.2 m distance were kept for the nozzle from the front and back side, respectively. The ambient depth, width, and distance of the nozzle tip to the lower boundary satisfy the deep flow regime criteria ($\frac{dFr_d}{H} < 0.42$, Abessi and Roberts 2015) and the free jet behavior of the single jet (Ramezani et al. 2020). A grid of 1,461,769 cells was generated with SnappyHexMesh. To achieve higher accuracy, four levels of refinement have been taken. Each level is shown in Fig. 1. The cells around the nozzle have the smallest size for catching all eddies to reach better results. For the wall boundaries, the no-slip condition is set for the velocity, and the slip condition is imposed on the top surface of the computational domain. In addition, for wall boundaries, the fixedFluxPressure boundary condition was applied to the pressure. The flow characteristics used for the simulations are specified in Table 1. The nozzle inlet's boundary conditions are:

$U_x = U_0\, cos(\theta)\,, U_y = U_0\, sin(\theta)\,, U_z = 0, C = C_0$, fixedValue

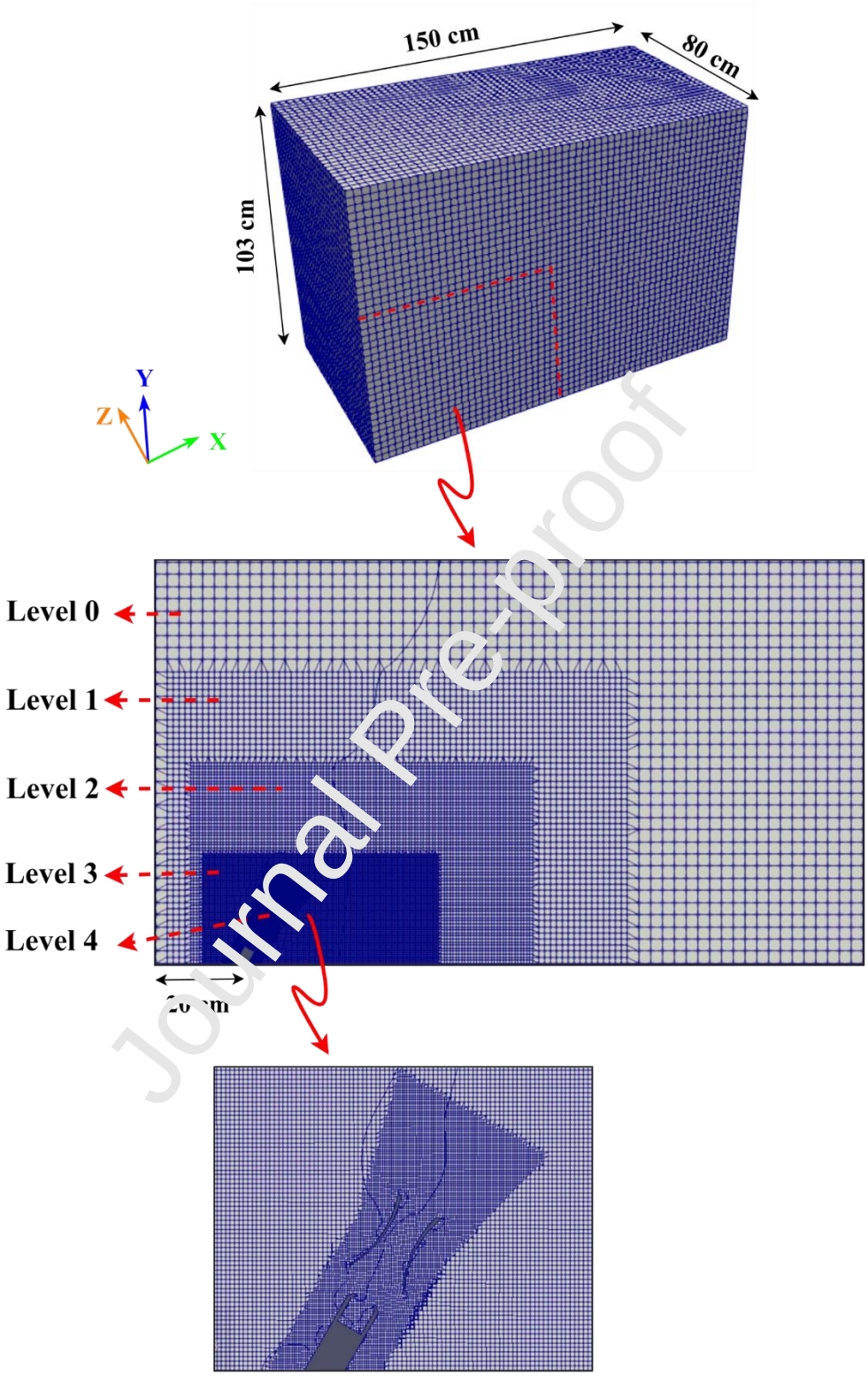

Fig. 1. The geometry and computational grid of the simulated setup

The resolution of the computational grid has a significant impact on the LES results. The LES indices of Resolution Quality (LES_IQ_k) is a common criterion to assess the resolution quality of

the LES model. It is known as the ratio of the resolved to the total turbulent kinetic energy (TKE) and is expressed as:

$$M = \frac{k_{Res}}{k_{Res} + k_{SGS}} \quad (8)$$

In the above equation, k_{Res} and k_{SGS} are the resolved and sub-grid scale components of turbulent kinetic energy, respectively. M = 0.77−0.85 was recommended by Celik et al. (2005) to guarantee that the mesh resolution is fine enough. In addition, Pope (2000) suggests that a grid resolution is acceptable if the $M \geq 0.8$. In Fig. 2, M is shown in the diverging color map in the cross-section of the jet centerline. In this diagram, except a small region in front of the nozzle, the value of M remains above 0.8 across the entire domain.

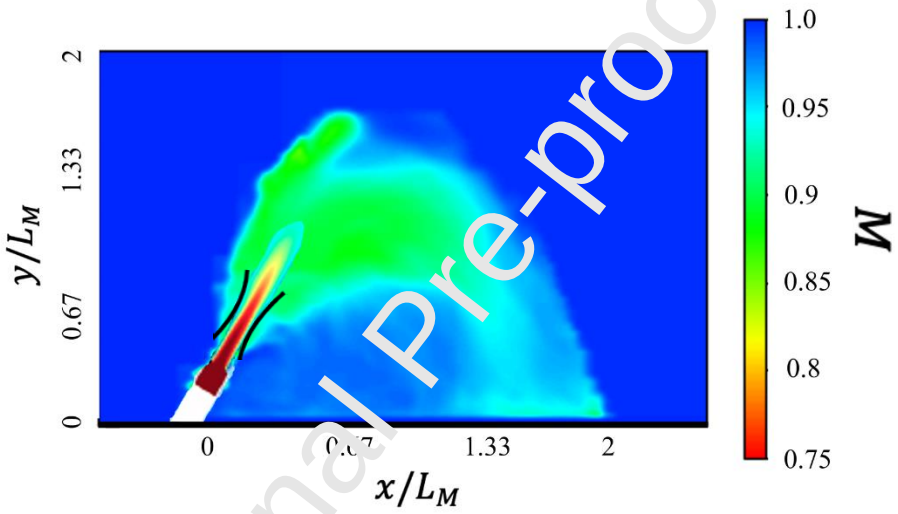

Fig. 2. The ratio of the resolved turbulent kinetic energy to the total turbulent kinetic energy

2.3 Experiments

In addition to the numerical simulations, a new series of experimental observations have been conducted in the Environmental Fluid Mechanics Laboratory of the Babol Noshirvani University of Technology. The experimental tank was placed in a dark room with dimensions of 3.5 × 5 meters. The tank features glass walls with dimensions of 1.8 m length, 1 m width, and 1 meter depth. A Venturi nozzle with an inlet diameter of 1 cm is placed at the bottom of the tank at 60°. The LIF system was used to measure the concentration field and spatial evolution of the discharge. Two fast-scanning mirrors were employed to produce a laser sheet that was placed over the centerline of the flow. The laser sheet was generated from a laser beam with a power of 0.2 watts and a wavelength of 514 nanometers. With a small volume of the fluorescent dye (Rhodamine 6G, Sigma-Aldrich, St. Louis, Missouri), the discharged effluent would fluoresce under the influence of the laser sheet. A CCD camera was used to record the emitted light at the rate of 100 frames per second in a long series of gray-scale images. The entire process was managed by a computer server equipped with an I/O board and controlling software. The images were continuously downloaded to the hard disk for later processing.

The captured images were adjusted and calibrated for laser attenuation and sensor response. Further details about the calibration process and the technique of extracting tracer concentration can be found in Tian and Roberts (2003) and Abessi et al. (2020). The process was first described by Daviero et al. (2001) and has since been used in many other investigations, e.g., Gungor and Roberts (2009), Fedele et al. (2015), and Abessi and Roberts (2017). The experimental setup and a photo of the observation in the laboratory for the dense discharge from the Venturi nozzle are displayed in Fig. 3. More details about the experimental parameters are given in Table 1.

Table 1. The flow characteristics in LES and Experimental simulations

Flow characteristic	LES	Exp
Discharge angle	60	60
Jet velocity	0.35 m/s	0.32, 0.35, 0.42, 0.47 m/s
Nozzle diameter	1cm	1cm
Effluent density	1019.27 kg/m^3	1019.28 kg/m^3
Ambient density	997.07 kg/m^3	996.99 kg/m^3
Modified acceleration (g')	0.218	0.219
Densimetric Froude number (Fr_d)	7.5	6.79, 7.5, 9.06, 10.57
Momentum-buoyancy length scale L_M (cm)	7.04	6.4, 7.04, 8.53, 9.95

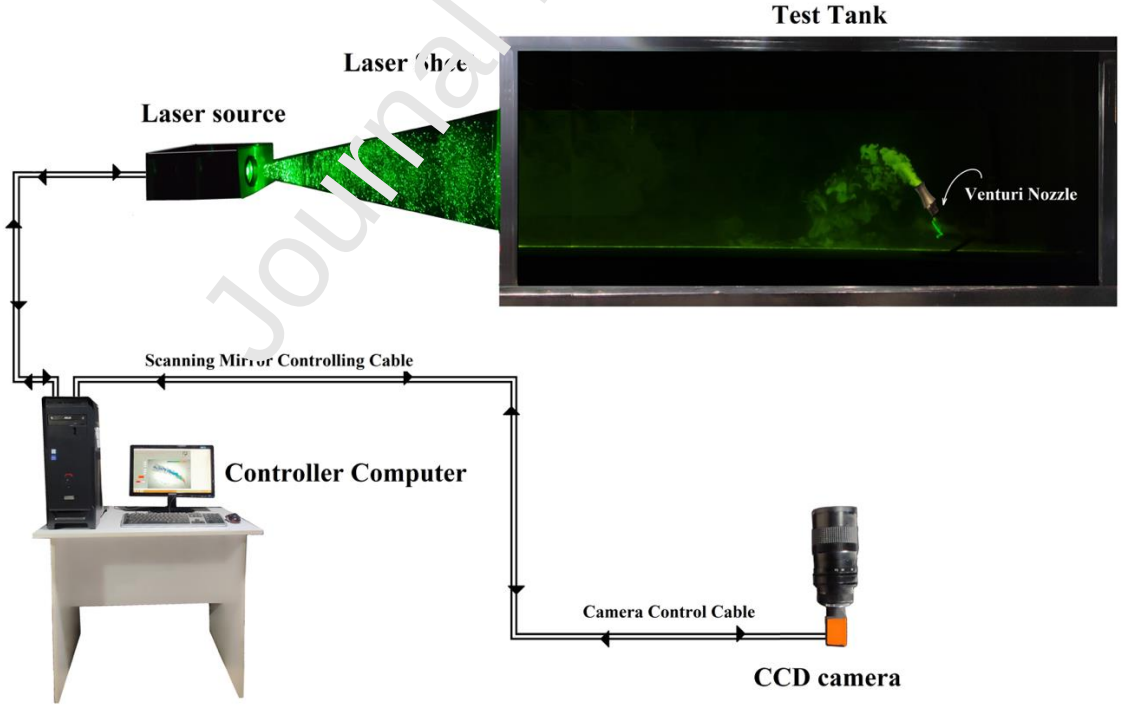

(a)

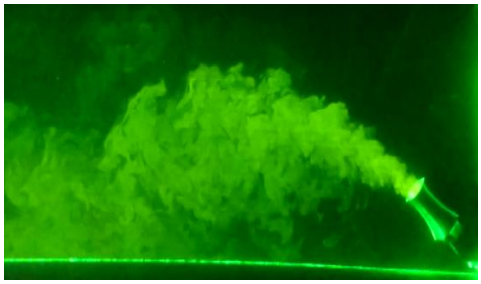

(b)

Fig. 3. (a) Schematic diagram of the experimental setup, (b) a photo of the experimental observation in the laboratory for the dense discharge from the Venturi nozzle

2.4 Experimental Errors

The LIF system used here in this study is similar to that previously developed and used by Tian and Roberts (2003). Errors in this system can be caused by the measurement uncertainties and optical misalignments. The sources of errors in measurements stem from uncertainties in various factors like flow rate, ambient and effluent density calculation, image magnification, tracer capture, and concentration calculation in the process of imaging, calibration, and corrections. Alignment errors refer to minor uncertainties in the positions of mirrors, lenses, and the camera. Significant efforts were undertaken to reduce these uncertainties substantially, to achieve dependable and consistent outcomes (Tian and Roberts 2003). The error of the the LIF system was reported by Tian and Roberts (2003) and is summarized below:

- Precision rotameter error: 3% (manufacturer-provided)
- Ambient and effluent densities measured with an accuracy of ±0.0001 g/cc
- Image magnification error: 1%.
- Image digitization error: 2%
- Calibration constant uncertainty: About 4% (due to dye solution and image capture errors)
- Additional errors introduced by the lens and attenuation corrections: 1% for unstratified environments and 4% for stratified environments

Altogether, this system will have a 5% error in concentration measurement for the investigated stagnant environments.

2.5 Dimensional Analysis

The schematic side view of an inclined dense discharge through a Venturi nozzle in stagnant water is shown in Fig. 4. The dimensions of the study nozzle are also depicted in Fig. 5. Venturi nozzles have found their primary application in the transfer of flow standards, uniform mixing of solutions in large tanks, improving the circulation of turbulent flow, and restricting maximum flow. Although initially used by the aerospace industry, Venturi nozzles are now extensively used in various industrial applications, such as automotive, energy, and metering. They were designed based on Bernoulli's theory to reduce fluid pressure when fluid flows through the inlet

cone. Due to the pressure differential, the pumped flow draws surrounding fluid into the jet through the Venturi's flow-through chamber. The additional liquid flow mixes with the discharge flow, and this decreases flow concentration through a sort of pre-dilution while also decreasing flow pressure and momentum. Hydraulic pressure at the Venturi nozzle inlet ranges from 0.5 to 4 bar and such a high pressure leads to the pressure differential that is crucial for the operation of the Venturi nozzles. The pressure differential between the inlet and the discharged flow varies with the operating liquid flow and increases with the rise in the flow rate. As a result, the liquid ratio varies, and the Venturi nozzle can pull in 2-4 gallons of surrounding fluid for every 1 gallon pumped through the nozzle. In this study, the effluent discharges from a round nozzle with a diameter of $\boldsymbol{d}$ (equal to 1 cm) to an inlet cone with a discharge diameter of $\boldsymbol{D}$ (equal to 3.5 cm). Therefore, the jet's initial velocity, $\boldsymbol{U_0}$, decreases to a lower velocity, $\boldsymbol{u}$, at the tip of the inlet cone. For brine discharges, jet density $\boldsymbol{\rho_0}$ is more than the density of ambient water $\boldsymbol{\rho_a}$, and the flow discharges at the initial angle of $\boldsymbol{\theta}$ to the horizontal plane. Like simple dense jets, the flow in a Venturi nozzle rises due to its initial momentum until it reaches the terminal rise height, $\boldsymbol{y_t}$, at the horizontal distance of $\boldsymbol{x_t}$, and then sinks toward the sea floor due to negative buoyancy. It eventually reaches the sea floor at the horizontal distance of $\boldsymbol{x_i}$ and continues to spread on the bed as a density current. The x_r is the return point and shows the location where the flow returns to the nozzle elevation. As shown in Fig. 4, the inlet nozzle tip (with 1 cm diameter) was assumed as the axis of the origin, and flow trajectory and geometrical characteristics were calculated from this point. Also, the dilutions at the return and impact point are referred to as return point dilution $\boldsymbol{S_r}$ and impact point dilution $\boldsymbol{S_i}$, respectively.

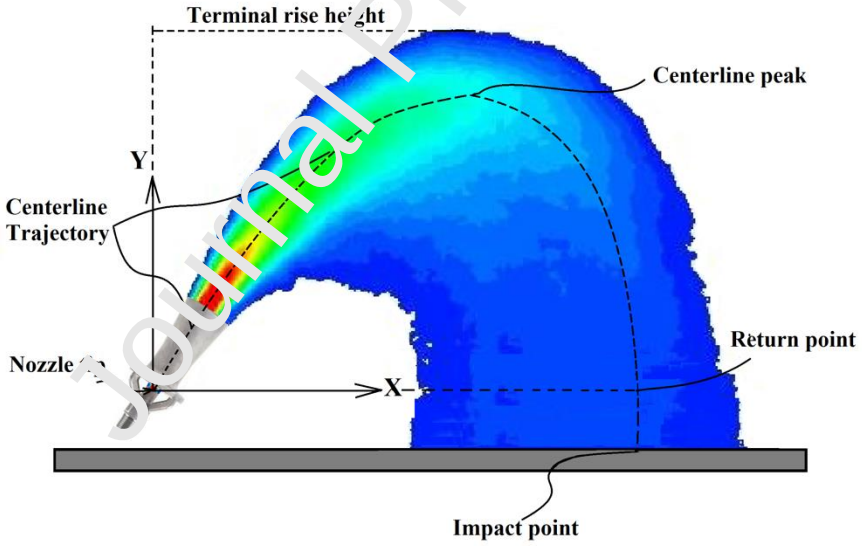

Fig. 4. A schematic side view of dense jet discharge through a Venturi nozzle

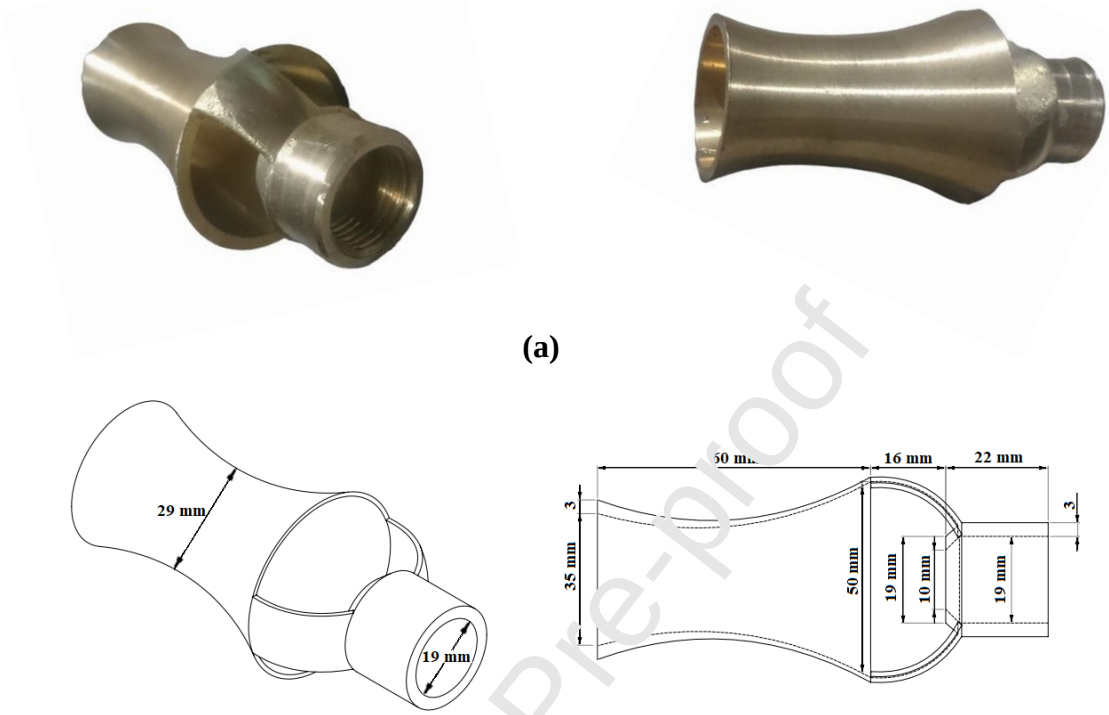

Fig. 5. (a) Studied Venturi nozzle profile in reality and (b) Schematic with dimensions

The concentration field of a dense jet is influenced by several factors, including jet discharge concentration C_0, the initial density difference $\Delta\rho$, U_0, d and θ. For the dense jet analysis, jet densimetric Froude number is a crucial factor. It quantifies the relationship between inertia and buoyancy for a submerged jet and denotes using the following equation:

$$Fr_d = \frac{U_0}{\sqrt{g'd}} \quad (9)$$

Where g' is the reduced gravitational acceleration and is calculated by:

$$g' = g(\frac{\Delta\rho}{\rho_a}) = \frac{g(\rho_0 - \rho_a)}{\rho_a} \quad (10)$$

The flow can be identified by the discharge initial volume flux (Q_0), momentum flux (M_0), buoyancy flux (B_0), and the discharge angle (θ) as described in the following equations:

$$Q_0 = \frac{\pi}{4} d^2 U_0 \quad (11)$$

$$M_0 = U_0 Q_0 \quad (12)$$

$$B_0 = g' Q_0 \quad (13)$$

Through dimensional analysis, we can demonstrate that a characteristic length (for example terminal rise height, y_t), can be formulated in 2 ways based on the discharge parameters as follows (Lai and Lee 2012):

$$\frac{y_t}{L_M} = f(\frac{L_M}{L_Q}, \theta) \quad (14)$$

Or

$$\frac{y_t}{dFr_d} = f(Fr_d, \theta) \quad (15)$$

Where, L_M represents jet-to-plume transition length scale that derived from the momentum and buoyancy fluxes. On the other hand, L_Q denotes a length scale associated with source discharge, extracted from the ratio of volume and momentum fluxes. These two parameters are expressed as:

$$L_M = \frac{M_0^{3/4}}{B_0^{1/2}} \quad (16)$$

$$L_Q = \frac{Q_0}{M_0^{1/2}} \quad (17)$$

L_M indicates the distance where the influence of jet momentum outweighs that of buoyancy, while L_Q signifies the range where the impact of source discharge is important. It is worth mentioning that L_M and L_Q can be correlated with the jet diameter (d) and the densimetric Froude number (Fr_d) as follows:

$$L_M = (\frac{\pi}{4})^{1/4} dFr_d \quad (18)$$

$$L_Q = (\frac{\pi}{4})^{1/2} d \quad (19)$$

In a similar manner, the return point dilution S_r and impact point dilution S_i, can be stated in an equivalent way as:

$$\frac{S_r}{Fr_d} = f(Fr_d, \theta) \quad (20)$$

$$\frac{S_i}{Fr_d} = f(Fr_d, \theta) \quad (21)$$

Therefore, L_M and Fr_d can be used for non-dimensionalizing the geometrical characteristics and dilutions of the dense discharge. Additionally, in the aforementioned equations, the jet diameter (d) is based on the inlet nozzle tip of the Venturi (1 cm here), as indicated in Fig. 4. Also, the nozzle is a simple round jet with a sharp edge.

3. Results and Discussion

3.1 General Observations

For the 60^o dense discharge, it took at least 20 seconds ($T^* = \frac{t}{M_0/B_0} \approx 6.5$) for the brine flow to reach the tank floor in the stagnant water (Galeshi et al. 2022). This is longer for the Venturi nozzle because of the pre-mixing effect that diminishes jet exit velocity. To have a stable result over the flow's instantaneous fluctuations, a mean flow must be obtained by time averaging the flow after reaching the quasi-steady state. This approach removes turbulent fluctuations and helps to better display mean flow behavior. Therefore, the simulation in this study continued until 70 s after the start time, and time averaging started after 30 s. The instantaneous and time-averaged contours in the Venturi nozzle for the normalized concentration (C/C_0) of the LES results are shown in Fig. 6. Due to the initial discharge momentum, the flow ascends like a jet until reaching the maximum level. The flow then descends due to its negative buoyancy and eventually impinges on the lower boundary. The location of the impact point is crucial because it is the first point where brine contacts benthic organisms. As expected, the flow concentration is significantly reduced from the source until it hits the sea floor. Shear entrainment due to the instabilities in the boundary is the dominant process for jet mixing in stagnant waters.

In Fig. 7, the instantaneous and time-averaged contours for the normalized concentration in a simple nozzle are illustrated in a diverging color map. As previously described by Tofighian et al. (2022) for showing the time evolution, time could be non-dimensionalized with the ratio of initial momentum to the buoyancy fluxes (M_0/B_0). Comparing the contours for the Venturi and simple nozzles shows significant changes in flow trajectory and jet lateral development for the Venturi discharge (Fig. 6) with respect to the simple nozzle (Fig. 7).

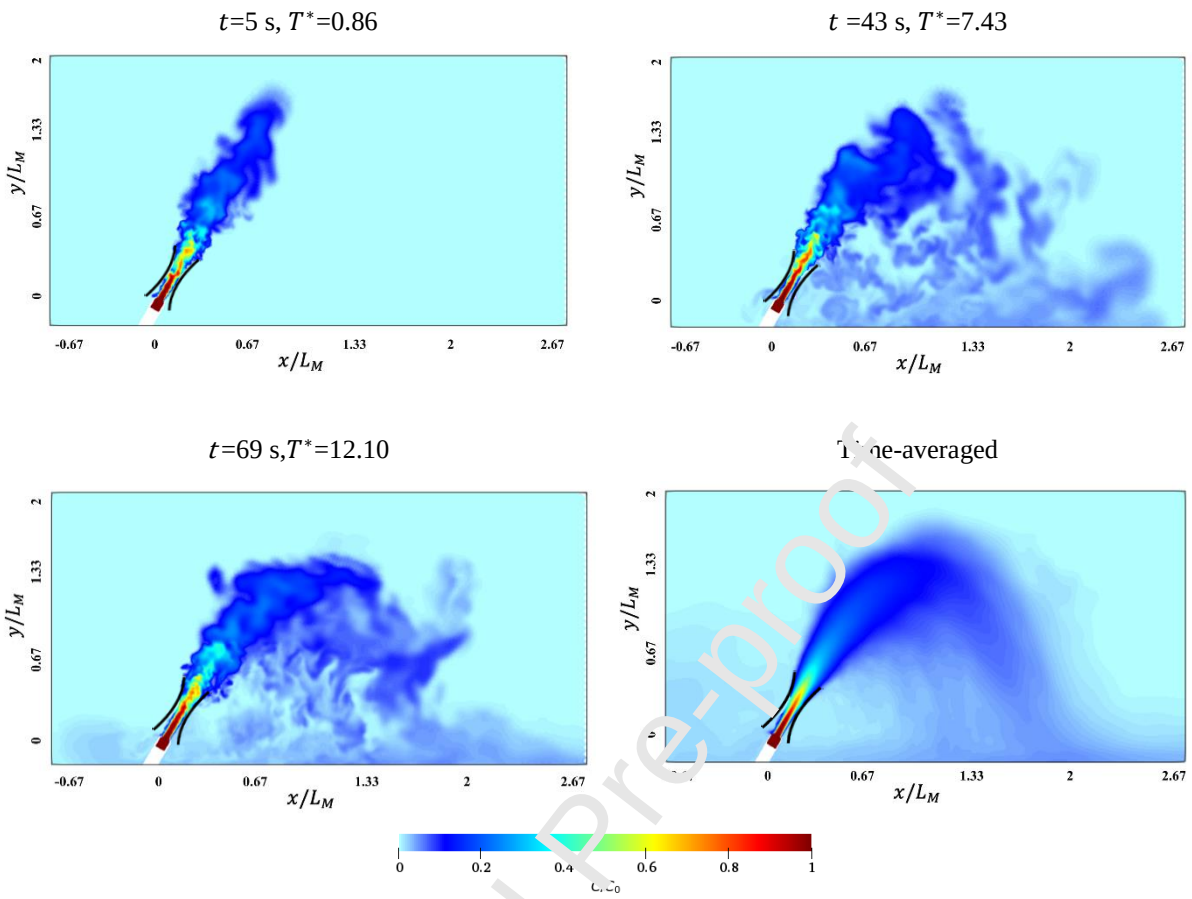

Fig. 6. LES results for flow development in time for Venturi nozzle at 60° and $Fr_d = 7.5$ for $T^* = \frac{t}{M_0/B_0} = 0.86, 7.43, 12.10,$ and time-averaged figure (left to right)

t=5 s, T^*=0.86 t=43 s, T^*=7.43

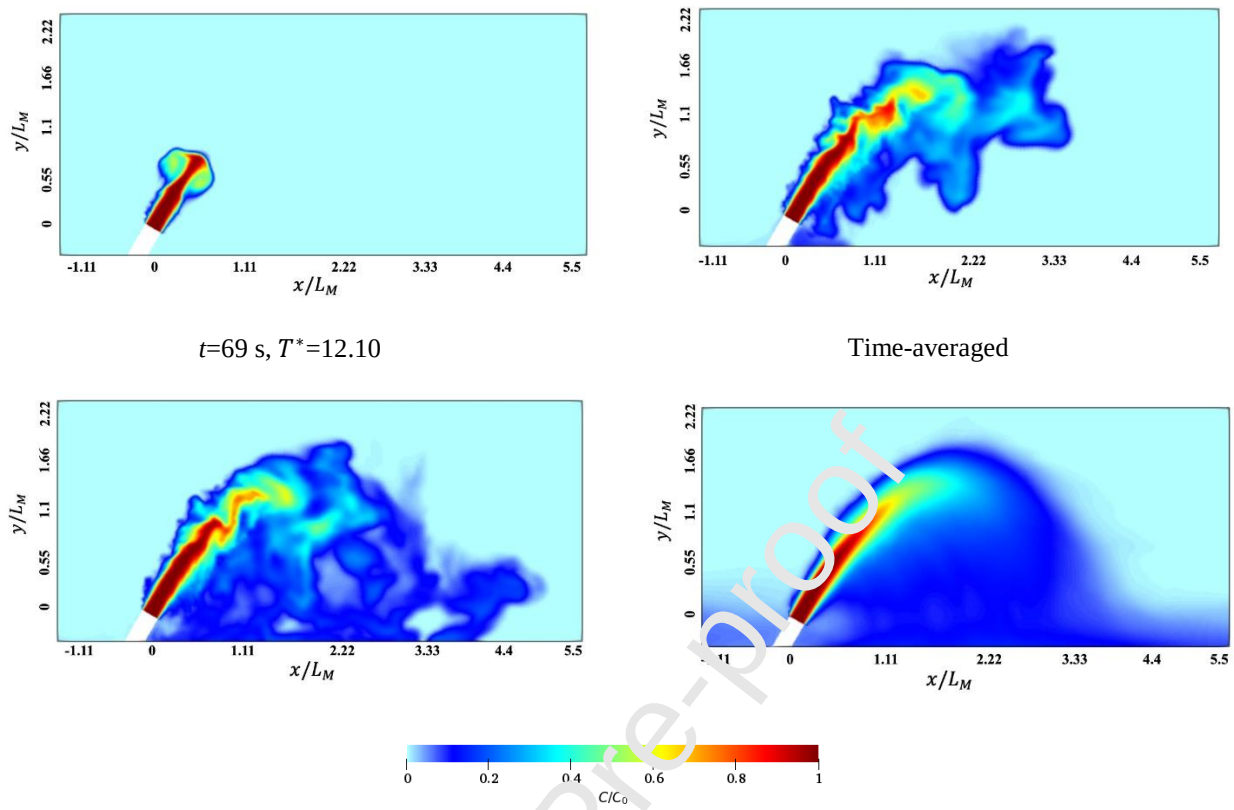

Fig. 7. LES results for flow development in time for simple nozzle at 60° and $Fr_d = 7.5$ for $T^* = \frac{t}{M_0/B_0} = 0.86, 7.43, 12.10,$ and time averaged figure (left to right)

The results of the LIF system for the Venturi nozzle experiments (VNExp) are also depicted in Fig. 8, showing the typical rising and falling behavior of a turbulent dense jet in different Froude numbers. The central planar tracer field is shown in false colors. The tracer concentration at each pixel was computed using the procedures outlined previously (Abessi and Roberts, 2014; Abessi et al. 2018). The planes are vertical and parallel to the jet direction and pass through the nozzle centerline in the x-y plane. As shown in Fig. 8, the centerline peak increases with the densimetric Froude number (from left to right in the figure) although it is non-dimensionalized by L_M. For the experimental results different from the numerical data, it is not possible to get a pictorial view of the tracer field inside the Venturi nozzle because the brass metal nozzle blocks the view of the camera. Therefore, the tracer field is only depicted from the point where the fluid leaves the nozzle cone, while the origin of the trajectory is still kept at the header tip, as shown in Fig 4.

Exp1, $Fr_d = 7.5$ Exp2, $Fr_d = 9.06$

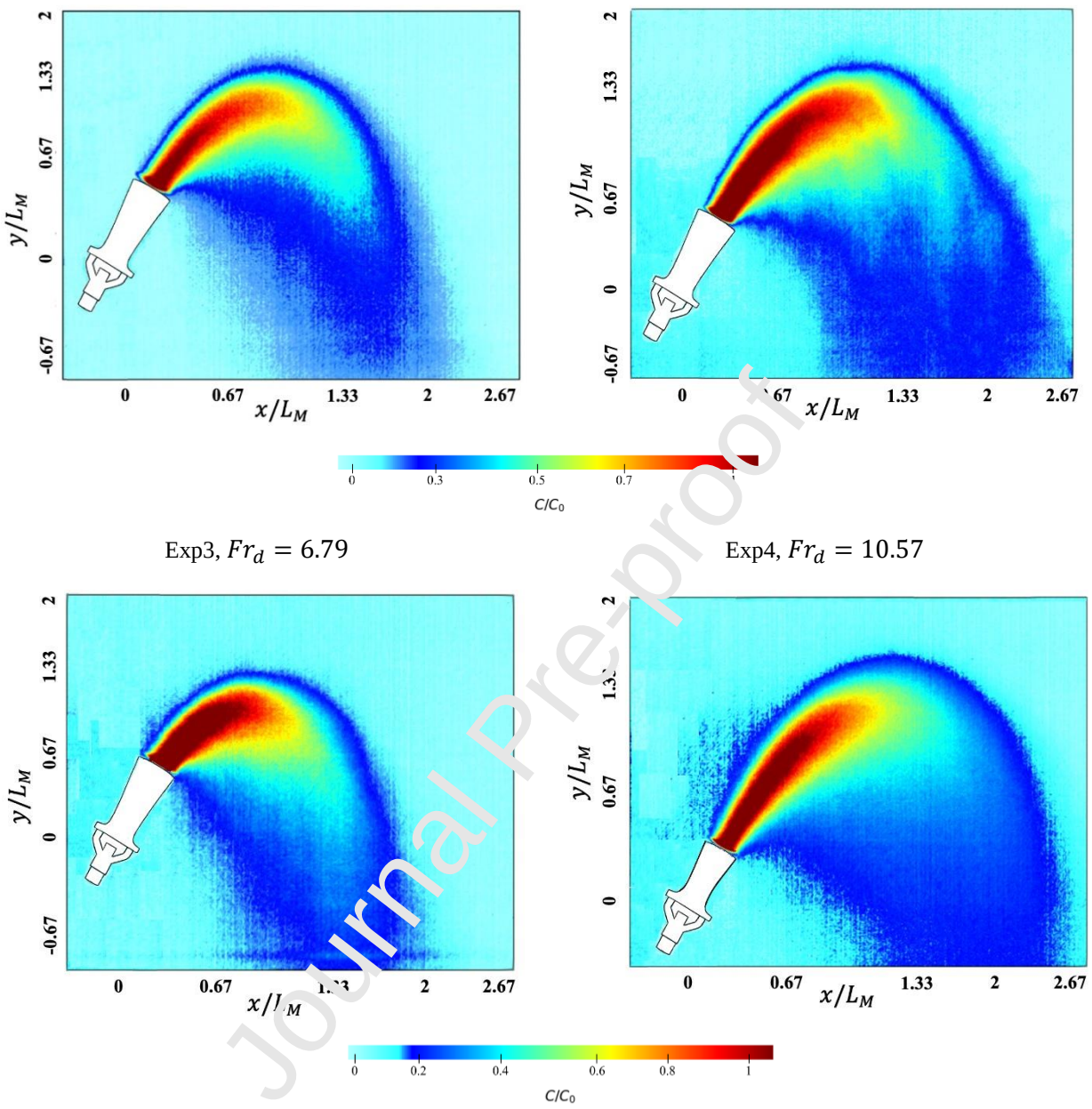

Fig. 8. Experimental results for central plane tracer concentrations; time-averaged results for $Fr_d = 6.79, 7.5, 9.06$ and 10.57 (top to bottom)

3.2 Jet Trajectory

The centerline trajectory or flow path is a major geometrical characteristic of any discharge. The trajectories were derived by connecting the locus of the maximum concentration or velocity at various cross-sections perpendicular to the flow. Concentration and velocity trajectories coincide generally with each other, as reported in Shao and Law (2010). However, the concentration trajectory falls more quickly than the other does (Zhang et al. 2016). The main geometrical characteristics, including jet terminal rise height, centerline maximum rise height, and the location of the impact point, can be predicted by determining the centerline trajectory. Fig. 9 shows the jet trajectories for both discharges with different Fr_d numbers when non-

dimensionalized with L_M for comparison. The numerical and experimental results were compared to previous studies. The results show that the LES trajectory for the simple nozzle is close to Kikkert (2006) and Palomar et al. (2012), while it is lower than Baum et al. (2019), and Galeshi et al. (2023) experimental data for the same nozzle type. As an interesting finding, the jet trajectory for the discharge from the simple nozzle was found to be significantly higher than the Venturi nozzle. As Fig. 9 shows, the LES results for the Venturi nozzle are in agreement with our LIF experiments, Exp 1 (Fr_d =7.5) and Exp 3 (Fr_d =6.79), and lie under the trajectory determined for Exp 2 (Fr_d =9.06) and Exp 4 (Fr_d =10.57).

The Venturi eductor needs very high exit velocities to reach the pressure difference required to produce the suction effect (Portillo et al. 2012). At higher velocities, the Venturi diffuser draws surrounding water in, through the nozzle's flow-through chamber and mixes an additional liquid flow with the pumped brine. The additional mixing varies with the pressure differential that forms in the Venturi device and grows as the discharge velocity rises. Such a discharge with high exit velocity places a limit on brine flow disposal. The inclined dense jet with a 60^o angle needs a very deep environment to avoid surface contact for high velocity. Therefore, a lower angle, 15^o, was used by Portillo et al. (2012) in the Maspalomas II desalination plant in the Canary Islands. It helped to prohibit surface impingement and to reach the required dilution at the same time. Using lower velocities for the brine discharge through the Venturi nozzles could be an option. This study, however, showed that lower velocities may lead to a complex non-self-similar behavior of the jet where the flow trajectory varies intricately with the Froude number (Fig. 9).

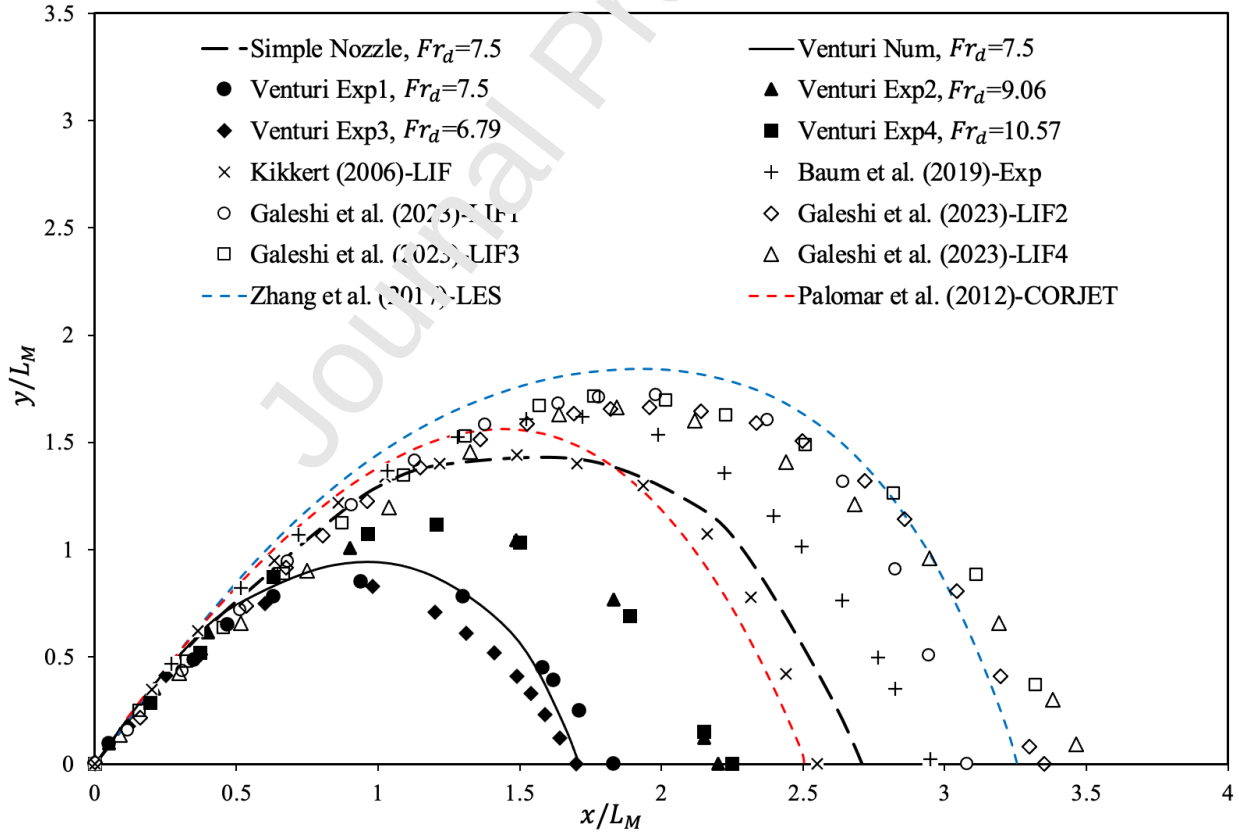

Fig. 9. Normalized centerline trajectories for 60° inclined discharge

3.3 Centerline Peak

The horizontal and vertical locations of the jet centerline peak (x_m, y_m) are derived from the jet centerline trajectory at the location of maximum rise height. For both numerical and experimental results, the location of the centerline peak is non-dimensionalized using L_M and plotted versus the discharge angle in Fig. 10. Previously reported data, such as Cipollina et al. (2005), Kikkert et al. (2007), Shao and Law (2010), and Lai and Lee (2012) are also plotted in the same figure. As shown in Fig. 10a and b, the LES prediction for a simple nozzle is in good agreement with Cipollina et al. (2005) and is slightly lower than Kikkert et al. (2007) and Lai and Lee (2012). The LES prediction for the Venturi nozzle is close to Exp 1 and Exp 3 and is lower than Exp 4. For the simple nozzle, the LES data are also lower than all reported experimental data. For the Venturi nozzle, as expected, the location of the flow centerline peak decreases significantly compared to a simple nozzle, and it inevitably decreases jet mixing and dilution. However, it provides the chance of using higher momentum along the near-field region before reaching the surface in shallow waters.

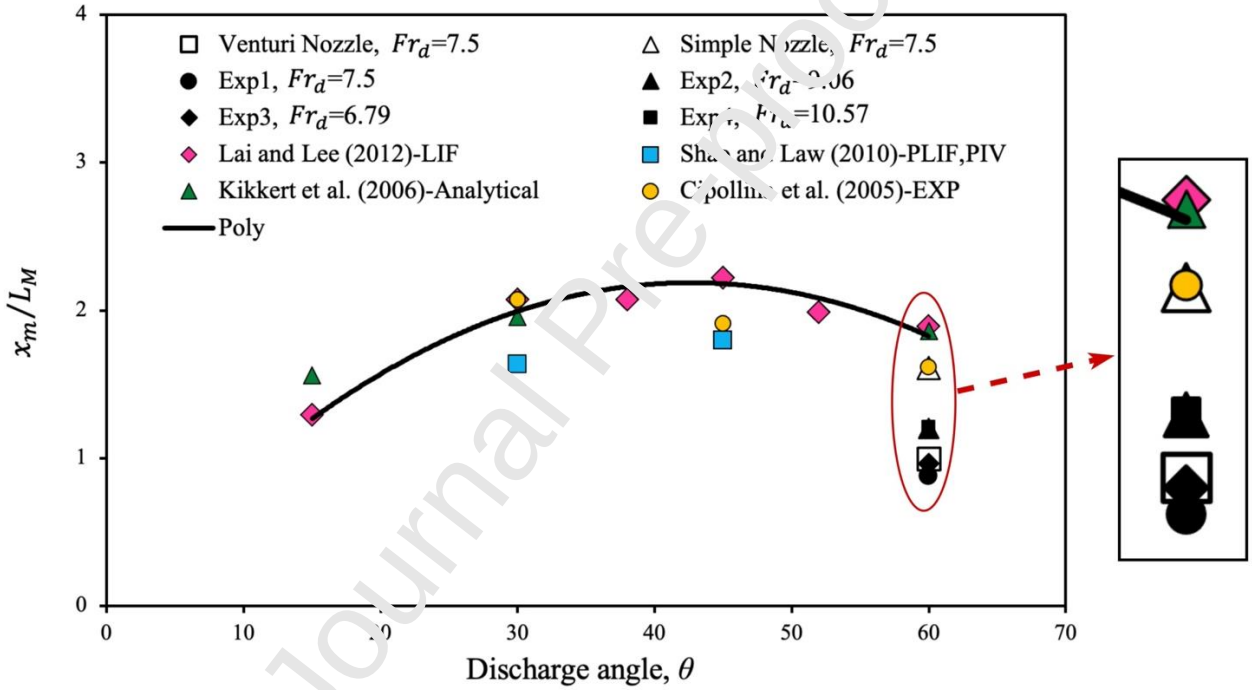

(a)

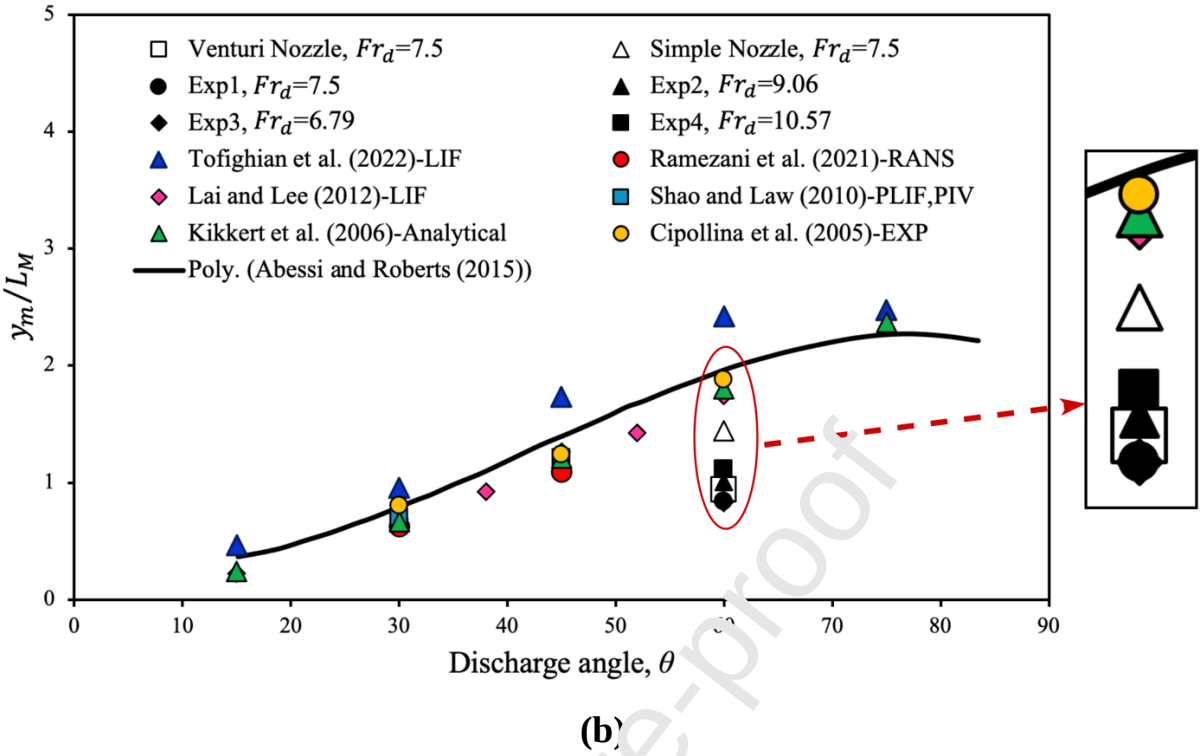

(b)

Fig. 10. Normalized centerline peak versus various nozzle angles (a) horizontal component (b) vertical component

3.4 Terminal Rise Height

Terminal rise height (y_t) is the jet's maximum possible height in the time-averaged figure of the concentration field and marks the point at which the momentum's vertical component significantly falls, becoming equal to zero. There is no common agreement among the previous studies regarding how to define the terminal rise height. Roberts et al. (1997) defined y_t as the location where the concentration is 10% of the transverse maximum concentration at the jet maximum height. According to Lai and Lee (2012), the 0.25 C_{max} concentration contour can be used to determine the visual boundary. The common integral model CORJET (Jirka 2008) employs cut-off levels of 3 and 25% to determine terminal rise height. Here, the cut-off level of 3% is used to determine the terminal rise height for LES and experimental results. Therefore, terminal rise height is determined using the time-averaged concentration field. In Fig. 11, the jet terminal rise height for numerical and experimental results is non-dimensionalized with L_M and plotted versus different angles. The predictions of the LES model for a simple nozzle are close to those from Lai and Lee (2012) and Kikkert et al. (2006). As shown in the figure, the numerical results for the Venturi nozzle are in acceptable agreement with Exp 3 and are slightly lower than Exp 4.

Jet terminal rise height is a crucial factor in defining the potential for reaching deep, surface contact, and shallow regimes. Dilution starts to decrease after the jet's upper side contacts the surface of the water (surface contact regime), because the entrainment from the jet's upside will cease. Mixing will be reduced further if the jet centerline reaches the water surface (shallow condition happens). This will limit the initial design goal for maximizing flow dilution at the impact point. It is the main reason why outfall designers try to keep the jet terminal rise height

below the water surface in all ebbs and floods. Using the Venturi eductor can help to reduce terminal rise height in water of limited depth, while it does not essentially lead to better dilution at critical points. This will be further explained in the following sections.

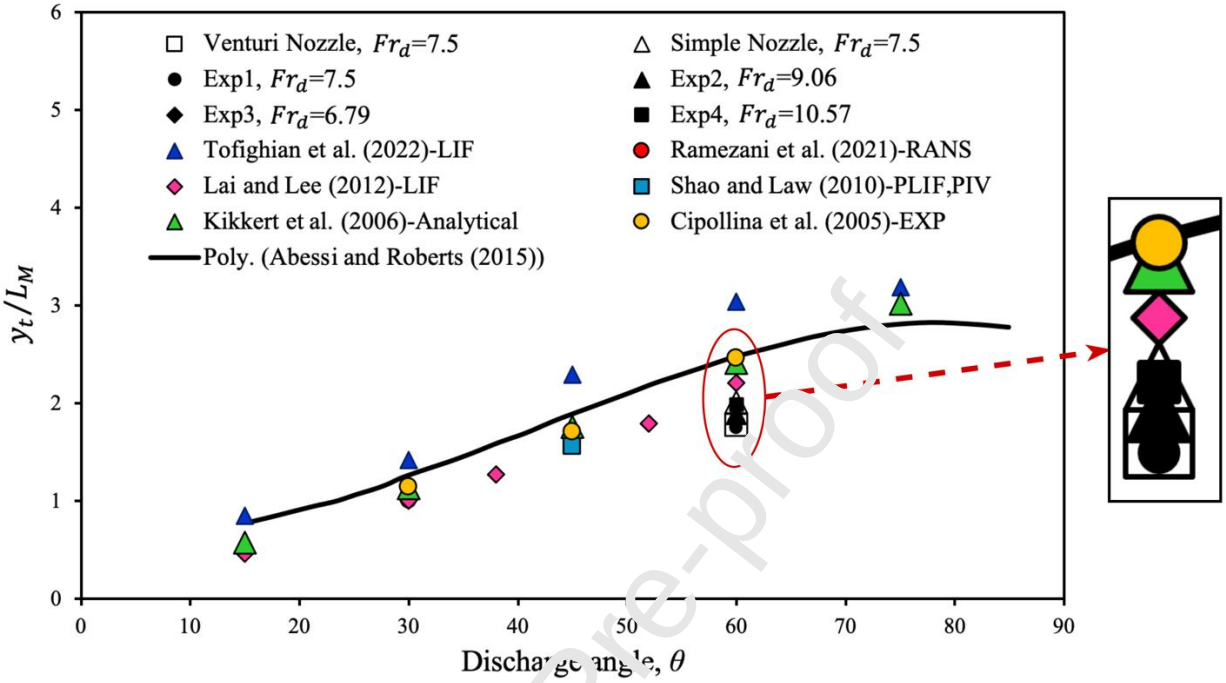

Fig. 11. Normalized terminal rise height versus various nozzle angles

3.5 Horizontal Distance to Return and Impact Point

The return point is the location where the dense jet crosses the nozzle tip elevation while it is falling in the jet's descending phase. If the nozzle tip is located above the sea floor, or if the bottom is sloped, this point highly differs from the impact point. The impact point is where the brine plume impinges on the sea floor and the minimum dilution appears along the lower boundary (Roberts et al. 1997). The impact point location is site-specific since it varies based on the nozzle height and bed slope. In previous studies, both return and impact points have been examined, e.g., Shao and Law (2010), Abessi and Roberts (2015), Crowe et al. (2016), Ramezani et al. (2021), and Tofighian et al. (2022). In Venturi nozzles, due to the discharge's higher elevation, flow properties (especially dilution) may be different from each other at these points. In Fig. 12a and b, the horizontal distance to the return and impact points is extracted from the numerical and experimental data, is non-dimensionalized with L_M, and is plotted versus the discharge angles. Like previously examined properties, the numerical results for the Venturi nozzle are in good consistency with Exp 3 and are relatively lower than Exp 4. In Figure 12a, it is evident that the results of the LES model for the simple nozzle closely align with the findings reported by Lai and Lee (2012) and Kikkert et al. (2007). However, it should be noted that these numerical results are notably higher than Cipolina et al. (2005). For the simple nozzle, the horizontal distance of the impact point is also lower than Abessi and Roberts (2015) and Tofighian et al. (2022). For the Venturi nozzle, however, the results for the return and impact point location were close to our experimental data.

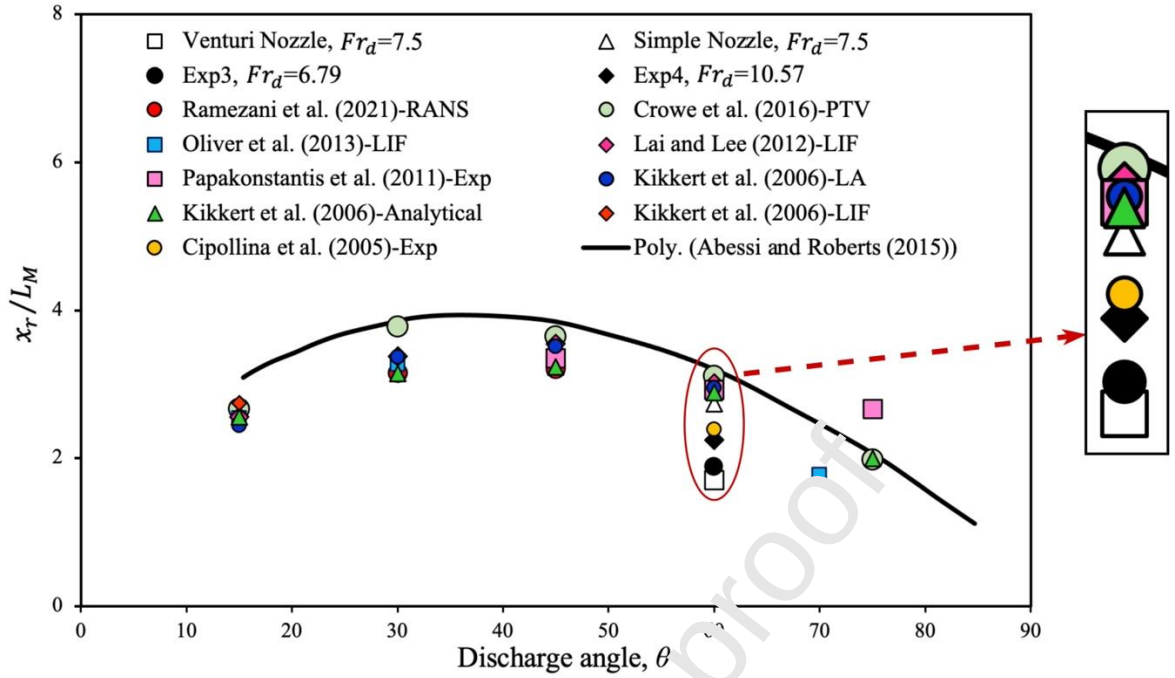

(a)

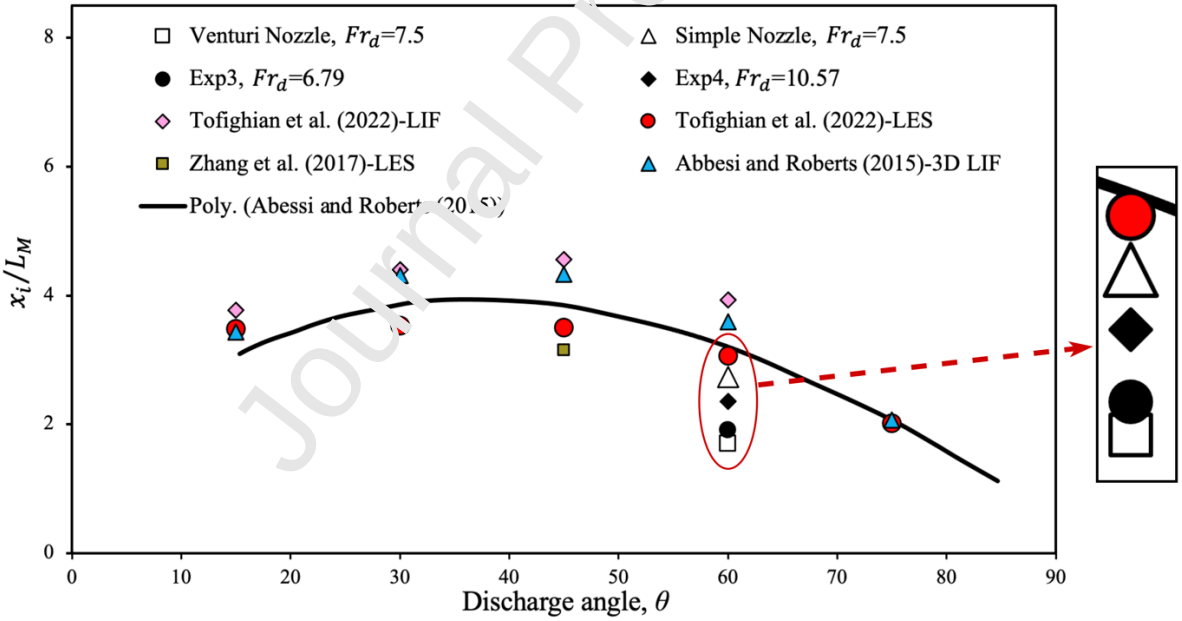

(b)

Fig. 12. Normalized horizontal distance of return point (a) and impact point (b) versus nozzle angles

3.6 Flow Width

Fig. 13 illustrates jet width (b) along the flow path (L_{Cl}) for both the inner (lower) and outer (upper) halves, which are normalized based on dFr_d. The determination of flow width was carried out separately for each section due to the asymmetric characteristics of the flow. If we

consider a Gaussian concentration distribution, the jet width is determined by measuring the distance from the centerline of the jet where the concentration level reaches $1/e$ of the centerline value. This ratio of jet width to path length is commonly used to describe the dispersion of dense jets. The calculated width was compared to data from prior studies conducted by Crowe et al. (2016), Ramakanth et al. (2016), and Galeshi et al. (2023). To facilitate comparisons, the positions of the centerline peak and return point were added within the same figure. In the case of the Venturi nozzle, the inner and outer widths closely match each other in the area around the source, whereas they begin to differ from one another thereafter. Furthermore, it was noticed that before and after the maximum rise height, the inner width increases and then decreases, while the outer width follows a different trend, steadily rising along the flow path. It can be observed from Fig. 13 that the inner and outer growth rates for the Venturi nozzle are much higher than those of the simple nozzle, indicating a larger lateral direction of the jet compared to both the simple nozzle and the values reported by Galeshi et al. (2023).

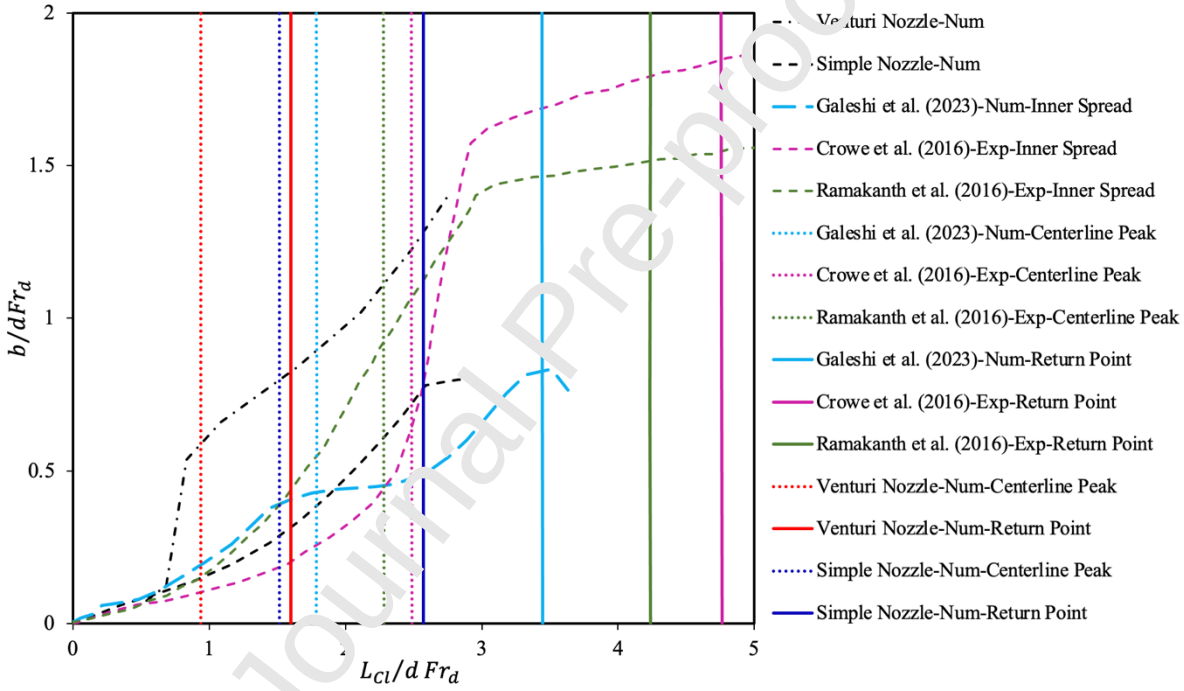

(a)

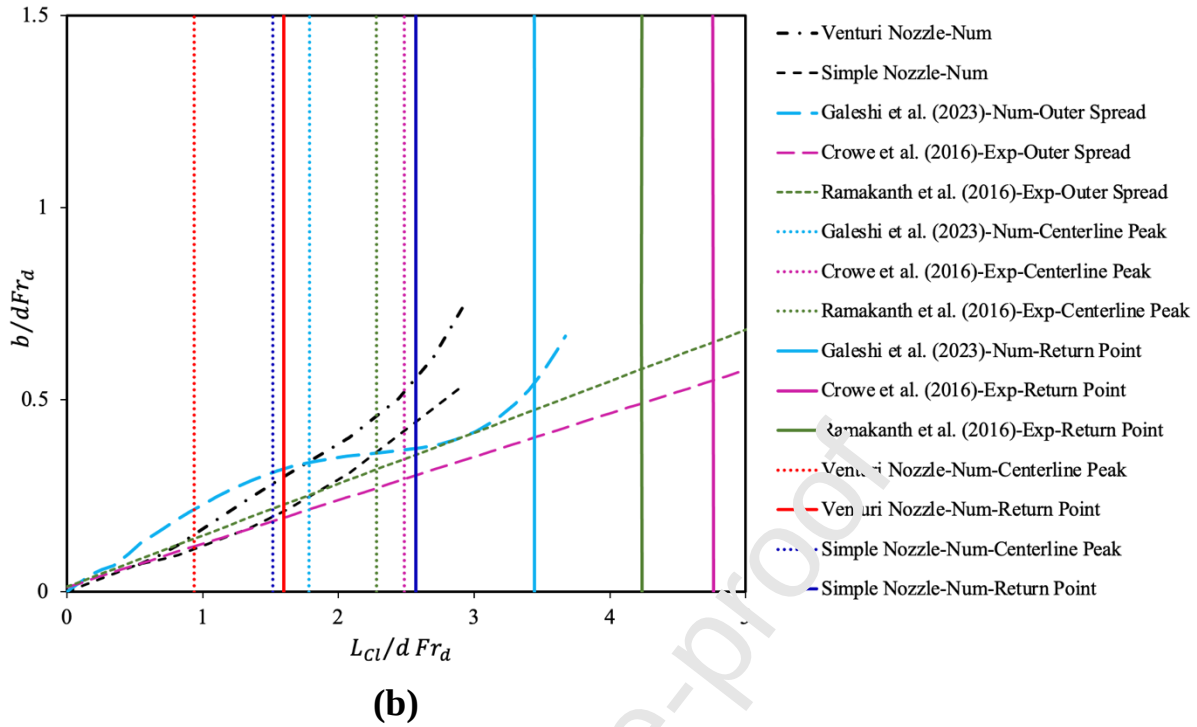

(b)

Fig. 13. Variation of concentration spread width along the trajectory: (a) inner spread (b) outer spread

3.7 Jet Mixing and Dilution

Dilution is defined as the initial concentration of tracer over local concentration at any point, C_0/C. Fig. 14a and b show dilutions at the return and impact point, which are normalized with Fr_d and plotted against the discharge angles. The dilution calculation at the return point is straightforward compared to that at the impact point because return point dilution is independent of the nozzle height and bed slope. Moreover, dilution at the impact point needs to be cautiously investigated due to the significant changes that occur in mixing and entrainment close to a bottom boundary. It is worth noting that benthic organisms have a limited ability to withstand salinity above the standards which makes the impact point the first location where strict standards of ambient water need to be met. The complex effects of the bottom boundary on flow mixing and dilution after the impact point have recently been addressed by Ramakanth et al. (2022) and Tofighian et al. (2022). In the post-contact phase of the flow on the bottom boundary, dilution still increases to its highest at some distance from the impact point. Then, entrainment falls due to the collapse in turbulent fluctuations and relaminarization at the end of the initial mixing zone (Roberts et al. 1997; Abessi and Roberts 2015).

As shown in Fig. 14a and b, the dilution predictions for the Venturi nozzle are consistent with Exp 3 and are considerably lower than Exp 4 and other studies. The dilution at the return point for the simple nozzle agrees with Kikkert et al. (2007) and is higher than Lai and Lee (2012). It was also lower than Crowe et al. (2016) and Oliver et al. (2013). In Fig. 14b, the impact point dilution for the simple nozzle is estimated lower than Abessi and Roberts (2015) but is close to Tofighian et al. (2022). For the Venturi nozzle, however, the numerical results were close to our LIF observations.

So, it can be concluded that, in the Venturi nozzles, the decrease in flow trajectory significantly diminishes jet dilution at the locations of the return and impact points. However, decreases in

dilution can be compensated for with proportional increases in jet velocity or discharge Froude number. These results indicate that in a receiving environment with limited depth, increasing the discharge Froude number to a magnitude comparable to that of a conventional jet can lead to slightly improved dilution at critical points, depending on the operational velocity. This enhancement enables the jet of the Venturi nozzle to reach the same elevation as a conventional jet typically achieves, with slightly better dilution.

To have a quantitative analysis of the flow trajectories, we summarized the main features of the flow in Table 2. The geometrical and dilution measurements are summarized in Table 2, along with the experimental, analytical, and numerical results of previous studies. Table 2 reveals that the LES results for the simple nozzle closely align with other reported data. However, in the case of the Venturi nozzle, both numerical and experimental models encountered challenges in predicting flow behavior. Nevertheless, they exhibited close agreement within the range of Froude numbers investigated.

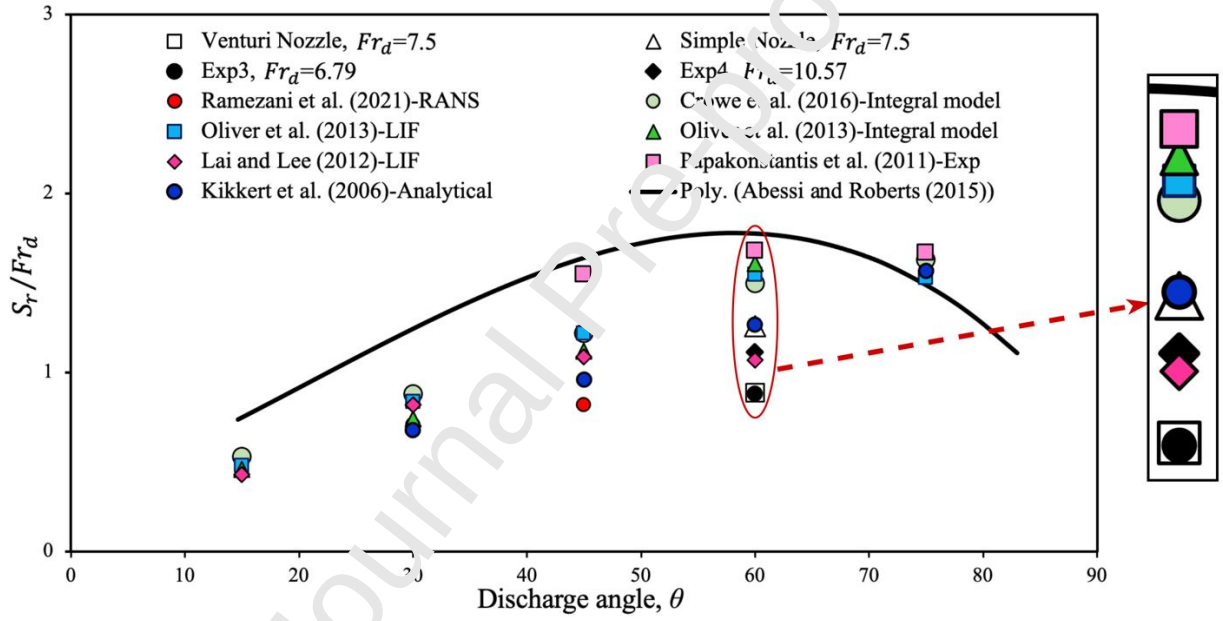

(a)

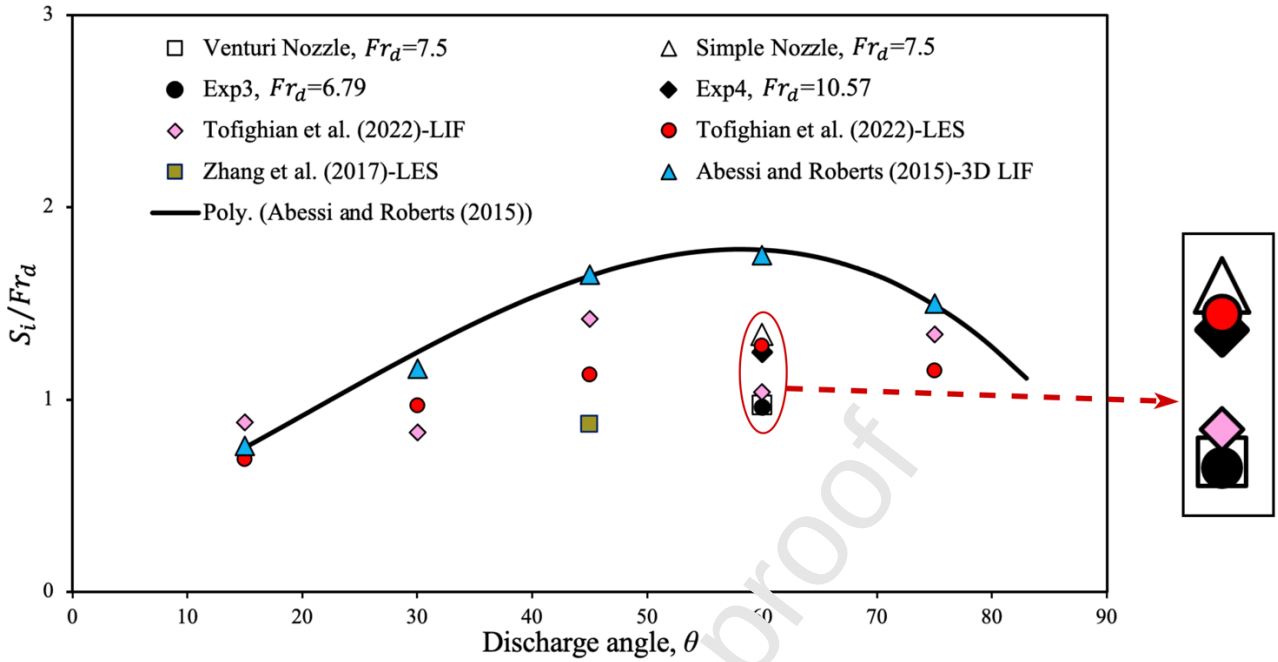

(b)

Fig. 14. Dilution at return point (a) and impact point (b) for various nozzle angles

Table 2. Summary of numerical and experimental results with comparison to previous data

Study	Description	x_m/L_M	y_m/L_M	y_t/L_M	x_r/L_M	x_i/L_M	S_r/Fr_d	S_i/Fr_d
Present Study, VNExp* 1	LIF	0.88	0.84	1.79	1.95	-	0.84	-
Present Study, VNExp 2	LIF	1.20	1.01	1.95	2.20	-	1.01	-
Present Study, VNExp 3	LIF	0.96	0.83	1.83	1.88	1.91	0.88	0.96
Present Study, VNExp 4	LIF	1.20	1.11	1.99	2.25	2.36	1.11	1.24
Simple Nozzle, Num	LES	1.61	1.44	2.01	2.73	2.80	1.26	1.34
Venturi Nozzle, Num	LES	0.99	0.94	1.78	1.70	1.80	0.89	0.97
Abessi and Roberts (2015), SNExp**	3D-LIF	-	-	2.69	-	3.59	-	1.75
Cipollina et al. (2005), SNExp	EXP	1.50	1.88	2.46	2.39	-	-	-
Kikkert et al. (2007), SNExp	LIF	1.85	1.86	2.60	-	-	-	-
Kikkert et al. (2007), SNExp	LA	-	1.69	2.42	2.95	-	-	-
Papakostantis et al. (2011), SNExp	Visual/Probe	-	1.78	2.28	2.92	-	1.68	-
Lai and Lee (2012), SNExp	LIF	1.89	1.74	2.20	3.01	-	1.07	-
Oliver et al. (2013), SNExp	LIF	-	1.71	2.34	2.93	-	1.55	-
Crowe et al. (2016), SNExp	PTV	-	1.81	2.36	3.11	-	1.27	-
Crowe et al. (2016), SNExp	Integral Model	-	1.67	-	2.83	-	1.50	-
Tofighian et al. (2022), SNExp	LIF	-	2.42	3.03	3.93	3.70	1.70	1.04
Tofighian et al. (2022), SNExp	LES	-	1.67	2.22	3.06	2.89	1.51	1.28
Galeshi et al. (2023), SNExp 1	LIF	1.77	1.72	2.56	3.53	-	2.14	-
Galeshi et al. (2023), SNExp 2	LIF	1.81	1.65	-	3.32	-	2.58	-
Galeshi et al. (2023), SNExp 3	LIF	2	1.72	-	3.42	-	1.95	-
Galeshi et al. (2023), SNExp 4	LIF	1.83	1.63	-	3.53	-	2.13	-

*Venturi Nozzle Experiment

** Simple Nozzle Experiment

As shown in Table 2, for the horizontal component of the normalized centerline peak (x_m/L_m), VNExp1 shows a 53% reduction compare to the Lai and Lee (2012) data for the simple nozzles. The LES results for the simple nozzle and Venturi nozzle are also 12% and 46% lower than Kikkert et al. (2006). The data for the vertical component of the normalized centerline peak (y_m/L_m) shows a 36% decrease for VNExp4 compare to Lai and Lee (2012). This parameter shows a reduction of 43% for LES results of the Venturi nozzle and 13% for the simple nozzle in comparison to Tofighian et al. (2022). Regarding the normalized terminal rise height (y_t/L_m), VNExp1 has a 53% reduction compared to the study by Lai and Lee (2012) for simple nozzles. Additionally, LES results for the simple nozzle and Venturi nozzle are 12% and 46% lower than Kikkert et al. (2006) in their findings for terminal rise height.

The normalized horizontal distance of the return point (x_r/L_m) for VNExp3 indicates a 37% difference compared to Oliver et al. (2013), and a 39% reduction is observed for the Venturi nozzle compared to Crowe et al. (2016). In contrast, the simple nozzle displays a smaller reduction of approximately 3.5% in comparison to Crowe et al. (2016). Furthermore, the dilution at this point is 3.6% greater for VNExp4 than Lai and Lee (2012), whereas for VNExp3, it is 17% smaller than the values reported by Lai and Lee (2012). In terms of dilution, the LES results indicate a reduction of 41% for the Venturi nozzle and 16% for the simple nozzle when compared to the findings of Tofighian et al. (2022).

4. Conclusions

The results of numerical simulations for quantifying flow behavior in brine discharge through the Venturi nozzle were compared with a new set of LIF experimental observations and with the previously reported data for the conventional nozzles. It is observed that the LES model developed for the Venturi nozzle effectively predicted flow behaviour. However, it underestimated flow geometrical and mixing properties compared to the experimental observations. Venturi eductors require extremely high exit velocities to reach the pressure difference required to produce the suction effect for the premixing. Such a high velocity makes it impossible to use the Venturi nozzle for steeply inclined discharges in coastal water. Therefore, lower exit velocities were investigated for 60^o dense jets. For the lower initial momentum, it is observed that the Venturi eductor causes the flow path and dilution to decrease for a fixed discharge velocity. However, this reduction can be compensated by proportionally increasing the discharge Froude number to achieve the same level of dilution as before. Therefore, this strategy's primary advantage lies in its ability to utilize the Venturi nozzle for dilution enhancement at the impact point by increasing discharge velocity under the same ambient conditions. This feature makes the Venturi nozzle an appropriate tool in coastal areas with shallow waters where outfall designers aim to avoid jet surface contact and are at the same time facing challenges in meeting required dilution levels. It is worth noting that further investigations involving variations in the discharge Froude number, exit velocities, number of nozzles, and the spacing of jets in a diffuser of the Venturi jets, and Venturi cone diameters may yield more comprehensive insight and reliable results.

References

Abessi, O., and Roberts, P. J. W. 2014. Multiport diffusers for dense dis- charges. J. Hydraul. Eng. 140 (8): 04014032. https://doi.org/10.1061 /(ASCE)HY.1943-7900.0000882.

Abessi, O., and Roberts, P. J. W. 2015a. Dense jet discharges in shallow water. J. Hydraul. Eng. 142 (1): 04015033. https://doi.org/10.1061 /(ASCE)HY.1943-7900.0001057.

Abessi, O., and Roberts, P. J. W. 2015b. Effect of nozzle orientation on dense jets in stagnant environments. J. Hydraul. Eng. 141 (8): 06015009. https://doi.org/10.1061/(ASCE)HY.1943-7900.0001032.

Abessi, O., and Roberts, P. J. W. 2018. Rosette diffusers for dense effluents in flowing currents. J. Hydraul. Eng. 144(1): 06017024. https://doi.org/10.1061/(ASCE)HY.1943-7900.0001403.

Abessi, O., 2018. Brine disposal and management—planning, design, and implementation. In: sustainable desalination handbook: plant selection, design and implementation.

Abessi, O., Roberts, P.J. and Gandhi, V., 2017. Rosette diffusers for dense effluents. Journal of Hydraulic Engineering, 143(4), p.06016029. https://doi.org/10.1061/(ASCE)HY.1943-7900.0001268

Abessi, O., Saeedi, M., Hajizadeh Zaker, N. and Khirkhah Gildeh, H., 2012. Flow characterization dilution in surface discharge of negatively buoyant flow in stagnant and non-stratified water bodies. Journal of Water and Wastewater, 22(4): 71-82.

Abessi, O., Rahmani Firoozjaee, A., Hamidi, M., Bassam, M.A. and Khodabakshi, Z., 2020. Three Dimensional Laser Scanning System for Illumination of Fluorescent flow for the Environmental Hydraulic investigations. Journal of Hydraulics, 14(4): 69-81.

Baum, M. J., Albert, S., Grinham, A., Gibbes, B. 2019. Spatiotemporal influences of open-coastal forcing dynamics on a dense multiport diffuser outfall. J. Hydraul. Eng. 145: 05019004. https://doi.org/10.1061/(ASCE)HY.1943-7900.0001622.

Cederwall, K. 1968. Hydraulics of marine waste water disposal. Rep. No. 42, Chalmers Institute of Technology, Gothenburg, Sweden.

Celik IB, Cehreli ZN, Yavuz I. 2005. Index of resolution quality for large eddy simulations. J Fluids Eng. 127: 949–958. https:// doi. org/ 10. 1115/1. 1990? 01

Cipollina, A., Brucato, A., Grisafi, F., Nicosia, S. 2005. Bench-scale investigation of inclined dense jets. J. Hydraul. Eng. 131: 1017–1022. https://doi.org/10.1061/(ASCE)0733-9429(2005)131:11(1017).

Crowe, A. T., Davidson, M. J., Nokes, R. I. 2016. Velocity measurements in inclined negatively buoyant jets. Environ Fluid Mech. 16: 503–520. https://doi.org/10.1007/s10652-015-9435-y.

Daviero, G. J., Roberts, P. J. W., Maile, K. 2001. Refractive index matching in large-scale stratified experiments. Experiments In Fluids. 31: 119–126. https://doi.org/10.1007/s003480000260.

Fedele, F., Abessi, O., Roberts, P. J. w. 2015. Symmetry reduction of turbulent pipe flows. J Fluid Mech. 779: 390–410. https://doi.org/10.1017/jfm.2015.423.

Fischer, H. B., List, E. J., Koh, R. C. Y., Imberger, J., and Brooks, N. H. 1979. Mixing in inland and coastal waters. Academic Press, New York.

Galeshi, A., Abessi, O., Yousefifard, M., and Firoozjaee, A. R. 2022. An experimental study on the process of mixing and dilution for the discharge of dense effluent. Journal of Hydraulics. 17(4). 10.30482/JHYD.2022.335691.1597.

Galeshi, A., Abessi, O., Yousefifard, M., and Firoozjaee, A. R. 2023. Inclined dense discharge in stagnant and wave environments: An experimental and numerical study. Ocean Engineering. 278:114045. https://doi.org/10.1016/j.oceaneng.2023.114045.

Gildeh, H. K., Mohammadian, A., Nistor, I., and Qiblawey, H. 2015a. Numerical modeling of 30° and 45° inclined dense turbulent jets in stationary ambient. Environ Fluid Mech. 15(3): 537–562. https://doi.org/10.1007/s10652-014-9372-1.

Gungor, E., and Roberts, P. J. W. 2009. Experimental studies on vertical dense jets in a flowing current. J. Hydraul. Eng. https://doi.org/10.1061/(ASCE)HY.1943-7900.0000106, 935–948.

Gutmark, E. J., and Grinstein, F. F. 1999. Flow control with noncircular jets. Annual review of fluid mechanics. 31(1): 239-272. https://doi.org/10.1146/annurev.fluid.31.1.239.

Hoekstra, A.Y. 2014. Water scarcity challenges to business. Nature climate change. *4*(5): 318-320.

Jiang, M., Law, A.W.K., and Song, J. 2019. Mixing characteristics of inclined dense jets with different nozzle geometries. Journal of Hydro-environment Research. *27*: 116-128. https://doi.org/10.1016/j.jher.2019.10.003.

Jirka, G. H. 2008. Improved discharge configurations for brine effluents from desalination plants. J. Hydraul. Eng. 134(1): 116–120. https://doi.org/10.1061/(ASCE)0733-9429(2008)134:1(116).

Kikkert, G. A. 2006. Buoyant jets with two and three-dimensional trajectories. University of Canterbury.

Kikkert, G. A., Davidson, M. J., and Nokes, R. I. 2007. Inclined negatively buoyant discharges. J. Hydraul. Eng. 133(5): 545–554. https://doi.org/10.1061/(ASCE)0733-9429(2007)133:5(545).

Kim, W. W., and Menon, S. 1995. A new dynamic one-equation subgrid-scale model for large eddy simulations. In 33rd Aerospace Sciences Meeting and Exhibit. (p356). https://doi.org/10.2514/6.1995-356.

Lai, C. K. C., and Lee, J. H. W. 2012. Mixing of inclined dense jets in stationary ambient. J. Hydro Environ. 6(1): 9–28. https://doi.org/10.1016/j.jher.2011.08.003.

Lee, A. W. T., and Lee, J. H. W. 1998. Effect of lateral confinement on initial dilution of vertical round buoyant jet. *J. Hydraul. Eng.* 124(3: 263-279. https://doi.org/10.1061/(ASCE)0733-9429(1998)124:3(263).

Lee, J.H., Wilkinson, D.L., and Wood, I.R. 2001. On the head-discharge relation of a duckbill elastomer check valve. Journal of hydraulic research. *39*(6): 619-627. https://doi.org/10.1080/00221686.2001.9628291.

Mi, J., Nathan, G.J. and Luxton, R.E. 2000. Centerline mixing characteristics of jets from nine differently shaped nozzles. Experiments in Fluids. *28*(1): 92-94. https://doi.org/10.1007/s003480050012.

Oliver, C. J., Davidson, M. J., and Nokes, R. I. 2008. k-ε predictions of the initial mixing of desalination discharges. Environ Fluid Mech. 8(5–6): 617–625. https://doi.org/10.1007/s10652-008-9108-1.

Oliver, C. J., M. J. Davidson, and R. I. Nokes. 2013. Behavior of dense discharges beyond the return point. J. Hydraul. Eng. 139 (12): 1304–1308. https://doi.org/10.1061/(ASCE)HY.1943-7900.0000781.

Palomar, P., Lara, J.L. and Losada, I.J., 2012. Near field brine discharge modeling part 2: Validation of commercial tools. Desalination, *290*: 28-42. https://doi.org/10.1016/j.desal.2011.10.021.

Papakonstantis, I. G., Tsatsara, E. I. 2019. Mixing characteristics of inclined turbulent dense jets. Environ Process. https://doi.org/10.1007/s40710-019-00359-w.

Pope, SB., 2000. *Turbulent Flows*, Cambridge University Press, Cambridge. https://doi. org/ 10. 1017/ CBO9780511840531.

Portillo, E., Louzara, G., Ruiz de la Rosa, M., Quesada, J., Gonzalez, J.C., Roque, F., Antequera, M. and Mendoza, H. 2013. Venturi diffusers as enhancing devices for the dilution process in desalination plant brine discharges. Desalination and Water Treatment. 51(1-3): 525-542. https://doi.org/10.1080/19443994.2012.694218.

Ramakanth, A., Davidson, M.J. and Nokes, R.I. 2022. Laboratory study to quantify lower boundary influences on desalination discharges. Desalination. 529: 115641. https://doi.org/10.1016/j.desal.2022.115641.

Ramezani, M., Abessi, O., Firoozjaee, A. R. 2021. Effect of proximity to bed on 30° and 45° inclined dense jets: a numerical study. Environ Process. 8: 1141–1164. https://doi.org/10.1007/s40710-021-00533-z.

Ramezani, M., Abessi, O. and Rahmani Firoozjaee, A., 2020. Numerical Simulation of Dense Discharges from 30o Submerged Inclined Jet in Free and Bed-Affected Conditions. Journal of Hydraulics, 15(3), pp.75-91. https://doi.org/10.30482/JHYD.2020.228141.1454

Roberts, P. J. W., and Toms, G. 1987. Inclined dense jets in a flowing current. J. Hydraul. Eng. 113(3): 323–341. https://doi.org/10.1061/(ASCE)0733-9429(1987)113:3(323).

Roberts, P. J. W., A. Ferrier, and G. Daviero. 1997. Mixing in inclined dense jets. J. Hydraul. Eng. 123(8): 693–699. https://doi.org/10 .1061/(ASCE)0733-9429(1997)123:8(693).

Roberts, P.J. and Abessi, O., 2014. Optimization of desalination diffusers using three-dimensional laser-induced fluorescence. Report Prepared for United States Bureau of Reclamation School of Civil and Environmental Engineering Georgia Institute of Technology, Atlanta, 30332.

Shao, D., and A. W. K. Law. 2010. Mixing and boundary interactions of 30° and 45° inclined dense jets. Environ. Fluid Mech. 10(5): 521–553. https://doi.org/10.1007/s10652-010-9171-2.

Tian, X., and Roberts, P. J. W. 2003. A 3D LIF system for turbulent buoyant jet flows. Experiments in fluids. 35(6): 636–647. https://doi.org/10.1007/s00348-003-0714-x.

Tofighian, H., Aghajanpour, A., Abessi, O., and Ramezani, M. 2022. Simulation of inclined dense jets in stagnant environments: an LES and experimental study. Environmental Fluid Mechanics. 22(5): 1161-1185. https://doi.org/10.1007/s10652-022-09884-z.

Vafeiadou, P., Papakonstantis, I., Christodoulou, G. 2005. Numerical simulation of inclined negatively buoyant jets. In: The 9th international conference on environmental science and technology. September. pp 1–3.

Wang, J., Weaver, D.S. and Tullis, S. 2012. Simplified fluid structure model for duckbill valve flow. Journal of pressure vessel technology. 134(4). https://doi.org/10.1115/1.4005941.

Zeitoun, M. A., Reid, R. O., McHilhenny, W. F., and Mitchell, T. M. 1970. Model studies of outfall system for desalination plants. Research and Development Progress Rep. No. 804, Office of Saline Water, U.S. Dept. of the Interior, Washington, DC.

Zhang, S., Jiang, B., Law, A. W. K., and Zhao, B. 2016. Large eddy simulations of 45° inclined dense jets. Environ. Fluid Mech. 16(1): 101–121. https://doi.org/10.1007/s10652-015-9415-2.

Zhang, S., Law, A. W. K., Jiang, M. 2017. Large eddy simulations of 45° and 60° inclined dense jets with bottom impact. J Hydro Environ Res. 15: 54–66. https://doi.org/10.1016/j.jher.2017.02.001.

Zhiyin, Y., 2015. Large-eddy simulation: Past, present and the future. Chinese journal of Aeronautics. *28*(1): 11-24. https://doi.org/10.1016/j.cja.2014.12.007.

Credit author statement

Niki Soleimani Amiri: Conceptualization, Data curation, Visualization, Writing- Original draft preparation, Software **Ozeair Abessi**: Supervision, Conceptualization, Methodology, Data curation, Writing, Review & Editing. **Philip J. W. Roberts:** Methodology, Writing, Review & Editing, Formal analysis.

Declaration of interests

☒The authors declare that they have no known competing financial interests or personal relationships that could have appeared to influence the work reported in this paper.

☐The authors declare the following financial interests/personal relationships which may be considered as potential competing interests:

Highlights

Brine discharge from the Venturi nozzle was investigated

The behavior of 60° inclined jets in a stagnant environment was explored

Both experimental and numerical scenarios were simulated using the LIF and LES method

The results were compared to the conventional round nozzles in both cases